Many-Body Spin Excitations in Ferromagnets from First Principles

43

Christoph Friedrich, Mathias C. T. D. Müller, and Stefan Blügel

Contents

Abstract

Electronic spin excitations are low-energy excitations that influence the properties of magnetic materials substantially. Two types of spin excitations can be identified, single-particle Stoner excitations and collective spin-wave excitations. They can be treated on the same footing within many-body perturbation theory. In this theory, the collective spin excitations arise from the correlated motion of electron-hole pairs with opposite spins. We present the theory in detail and discuss several aspects of an implementation within the full-potential linearized augmented plane-wave method. The pair propagation is described by the transverse magnetic susceptibility, which we calculate from first principles employing the ladder approximation for the T matrix. The four-point T matrix is represented in a basis of Wannier functions. By using an auxiliary Wannier set with suitable Bloch character, the magnetic response function can be evaluated for arbitrary $\mathbf{k}$ points, allowing fine details of the spin-wave spectra to be studied. The energy of the acoustic spin-wave branch should vanish in the limit $\mathbf{k} \to \mathbf{0}$,

C. Friedrich (✉) · M. C. T. D. Müller · S. Blügel
Peter Grünberg Institut and Institute for Advanced Simulation, Forschungszentrum Jülich and JARA, Jülich, Germany
e-mail: c.friedrich@fz-juelich.de; s.bluegel@fz-juelich.de

W. Andreoni, S. Yip (eds.), *Handbook of Materials Modeling*,
https://doi.org/10.1007/978-3-319-44677-6_74

which is a manifestation of the Goldstone theorem. However, this condition is often violated in the calculated acoustic magnon dispersion, which can partly be traced back to the choice of the Green function. In fact, the numerical gap error is considerably reduced when a renormalized Green function is used. As an alternative simple correction scheme, we suggest an adjustment of the Kohn-Sham exchange splitting. We present spin excitation spectra for the elementary ferromagnets Fe, Co, and Ni as illustrative examples and compare to model calculations of the homogeneous electron gas.

1 Introduction

Electronic spin excitations span a large range of energies, from high-energy single-particle Stoner excitations to low-energy collective spin-wave excitations. Therefore, they are present at all temperatures and play an important role for the physical properties of magnetic materials. For example, the specific heat (Doniach and Engelsberg 1966), the macroscopic magnetization (Bloch 1930), and the magnetic susceptibility (Moriya 1985) exhibit a characteristic temperature dependence which can be attributed to the low-energy spin waves (magnons) with excitation energies ranging from a few meV up to a few hundreds meV. In low-dimensional magnets, spin-wave excitations can even destroy the long-range magnetic order completely. This happens in the absence of magnetic anisotropy at any finite temperature (Mermin and Wagner 1966). As the temperature increases, in addition to collective magnon modes, single-particle spin-flip processes, so-called Stoner excitations, become increasingly important. They further contribute to the temperature variation of the magnetization and give rise to a damping of the magnon states.

Spin excitations play a role in many fields of fundamental and technological interest. They can contribute to the scattering of a propagating electron or hole in a magnetic material, leading to a renormalization of the quasiparticle band dispersion (Hofmann et al. 2009; Schäfer et al. 2004) and reducing the inelastic mean free path of hot electrons (Hong and Mills 1999, 2000). In magnetic recording applications, the creation of spin waves that accompanies each switching process in the storage medium sets physical limits on data rates and areal recording densities. A strong damping helps in dissipating the energy contained in the spin waves. The spin wave bus, on the other hand, utilizes spin waves as a means for information transmission between distant nanoscale devices (Khitun and Wang 2005). The damping through the creation of Stoner excitations is an undesirable effect in this case, limiting the distance over which information can be transmitted. The power consumption of such a spin wave bus is expected to be considerably lower than in charge-based devices. Finally, it is believed that the electron-electron interaction can become attractive through the exchange of magnons, which is a possible mechanism for the creation of Cooper pairs in high-temperature superconductors (Dagotto 1994; Scalapino 1995).

In quantum mechanics, the spin excited states are eigenstates of the many-body Hamiltonian with a net spin flip with respect to the many-body ground state. The magnetic response function or dynamical spin susceptibility, defined as a two-particle Green function in many-body perturbation theory, exhibits resonances at the corresponding eigenenergies. In an infinite system, these resonances – or poles – are, in general, not discrete but form a continuous distribution when plotted over the eigenenergy. This *spectral function* is given mathematically by the imaginary part of the magnetic response function and can be measured in inelastic neutron scattering experiments (Lowde et al. 1983) where the circularly polarized magnetic field of an incoming neutron beam disturbs the local magnetization density of the sample material. The magnetic response function is thus a central quantity in the theoretical study of magnetic materials.

For a theoretical description of spin dynamics, various formalisms have been established. Most theoretical studies to date employ the Heisenberg model, which relies on a separation of the magnetic degrees of freedom and the fast motion of the electrons. This model is defined in terms of exchange parameters, which can be obtained, for example, from constrained density functional theory (Rosengaard and Johansson 1997; Kübler 2009; Halilov et al. 1997). Spin waves with long wavelengths can be calculated efficiently. Single-particle Stoner excitations are neglected, though, and the linewidths of the spin-wave resonances, which are inversely proportional to the magnon lifetimes, are inaccessible. Furthermore, the Heisenberg model is strictly justified only for systems with localized moments, such as systems with rare-earth magnetic ions, but not for materials which are magnetized by the exchange-driven polarization of the spins of itinerant electrons. While the Heisenberg model still yields reasonable results for long-wavelength excitations in itinerant-electron magnets, results for short-wavelength excitations are unsatisfactory. For example, the multiple branches or gaps in the magnon dispersion of 3*d* ferromagnets cannot be captured (Cooke 1976).

Many-body perturbation theory (MBPT) provides a more general theoretical framework that works for systems with localized moments and for metallic magnets alike. Single-particle Stoner and collective spin excitations appear simultaneously as poles in the transverse magnetic susceptibility, which can be interpreted as describing the correlated motion of an electron-hole pair coupled by an effective electron-electron interaction. First applications to real systems (Cooke 1973; Cooke 1976) employed a tight-binding description. Reasonable agreement with experiment throughout the Brillouin zone was obtained for the spin-wave dispersion of 3*d* ferromagnets. With a similar approach, Tang et al. (1998) examined the spin dynamics in ultrathin ferromagnetic films on nonmagnetic substrates.

Around the turn of the millennium, the first calculations based on ab initio electronic structure methods were carried out: Karlsson and Aryasetiawan (2000) employed MBPT but used a local model potential with an adjustable parameter instead of the nonlocal electron-hole interaction. Savrasov (1998), Buczek et al. (2009), Lounis et al. (2010), and Rousseau et al. (2012) performed calculations

within time-dependent density functional theory (TDDFT). Kotani and van Schilfgaarde (2008) studied (anti-)ferromagnets based on quasiparticle self-consistent *GW* calculations (Faleev et al. 2004), where the effective interaction was determined from a magnetic sum rule. In 2010, Şaşıoğlu et al. (2010) reported a treatment within MBPT where the screened Coulomb interaction was explicitly calculated from the random-phase approximation (RPA) rather than using a model potential or a parameter fixed by a sum rule. Still an ad hoc scaling of the screened interaction was required to fulfill the Goldstone condition. Good agreement of the calculated magnon dispersions in 3*d* ferromagnets with experiment was achieved in both approaches, MBPT and TDDFT.

In the present chapter, we give a detailed presentation of the theoretical many-body treatment of spin excitations within MBPT. We adopt a very general viewpoint that encompasses excitations with and without a spin transfer, so neutral excitations – e.g., excitons, which play an important role in optical absorption – will appear as a special case. In Şaşıoğlu et al. (2010), a practical computational scheme was developed to study excitation spectra of magnetic materials from first principles, in close relation to the formalism of Aryasetiawan and Karlsson (1999). To study collective magnon excitations, we include vertex corrections in the form of ladder diagrams, which describe the coupling of electrons and holes with opposite spins via the screened Coulomb interaction. In analogy to the many-body T matrix defined by Strinati (1988) for optical absorption, we use the same term for the corresponding quantity that appears in the Green-function formalism for the transverse magnetic response function. In order to reduce the numerical cost for the calculation of the four-point T matrix, we exploit a transformation to maximally localized Wannier functions (MLWFs), which provide a more efficient basis to study local correlations than extended Bloch states (Marzari and Vanderbilt 1997; Souza et al. 2001; Freimuth et al. 2008). Our implementation is based on the full-potential linearized augmented plane-wave (FLAPW) method.

Section 2 gives a detailed account of the theoretical framework. The numerical implementation is described in Sect. 3. In particular, we discuss how the magnetic response function can be calculated for any Bloch vector, even if this Bloch vector is not an element of the **k**-point set. This allows the calculation of smooth dispersion curves while keeping the **k**-point set small. Section 4 is devoted to the discussion of the violation of the Goldstone theorem. This theorem stipulates the existence of an acoustic magnon branch with vanishing excitation energy in the long-wavelength limit. In numerical calculations, the excitation energy often remains finite in this limit. We show – both numerically and mathematically – that this violation is due to an inconsistency in the choice of the single-particle Green function. In Sect. 5, we present illustrative magnetic excitation spectra obtained for the elementary ferromagnets bcc Fe, fcc Co, and fcc Ni. For more practical applications of this method, we refer the reader to Friedrich et al. (2014) and Şaşıoğlu et al. (2010, 2013). In Sect. 6, we summarize our conclusions. Unless otherwise indicated, Hartree atomic units are used throughout.

2 Theory

When a many-electron system is perturbed by a time-dependent external **B** field, originating, for example, from a neutron beam impinging on a magnetic sample, the system reacts by a change of the electronic density. This electronic redistribution is different for spin-up and spin-down electrons, since the **B** field couples to the electrons' spin, and, to a first approximation, it is the spin density that changes, while the total density remains the same. Therefore, we consider the magnetic response function

$$R^{ij}(\mathbf{r}_1 t_1, \mathbf{r}_2 t_2) = \frac{\delta \sigma^i(\mathbf{r}_1 t_1)}{\delta B^j(\mathbf{r}_2 t_2)}\,, \tag{1}$$

which gives the linear change of the spin density at the position $\mathbf{r}_1$ and time t_1 with respect to changes in the external **B** field at $\mathbf{r}_2$ and t_2. Here, σ^i and B^j are the vector components ($i, j = x, y, z$) of the spin density $\boldsymbol{\sigma}$ and the **B** field. We additionally allow for $i = 0$ and $j = 0$, where σ^0 is the total electronic density and B^0 is an external scalar potential. For example, $R^{00} = \delta\sigma^0/\delta B^0$ then corresponds to the density response function. Equation (1) thus defines a 4×4 tensor of response functions that are all nonzero in general.

The magnetic response function exhibits resonances (analytical poles) at the spin excitation energies of the unperturbed many-body system, corresponding to the eigen oscillations of the spin system. These "eigen oscillations" are, in general, not discrete and show a spectral distribution given by the imaginary part of the magnetic response function. In order to capture all possible oscillations of the spin system, Eq. (1) defines a microscopic response function in the sense that the perturbing field – and also the response of the electronic (spin) density – can have an arbitrary shape in space. In particular, it can exhibit any wavelength down to interatomic distances. Its determination requires an ab initio description of the electronic structure and a high-level quantum mechanical treatment of the correlated motion of the electrons.

We employ a method based on MBPT similar to the one of Aryasetiawan and Karlsson (1999). However, we do not employ Matsubara frequencies but a formulation at absolute zero that yields the magnetic excitation spectra directly for real frequencies. An implementation within an all-electron Wannier-function formulation was published in Şaşıoğlu et al. (2010) and Friedrich et al. (2014). In the following, we develop the theory in detail.

To simplify the notation, space and time arguments $\mathbf{r}_1 t_1, \mathbf{r}_2 t_2, \ldots$ are abbreviated by the corresponding index 1, 2, ... The ground-state spin density distribution is given by the expectation value of the spin density operator

$$\sigma^i(1) = \sum_{\alpha,\beta} \sigma^i_{\alpha\beta} \langle \Psi_0 | \psi^\dagger_\alpha(1) \psi_\beta(1) | \Psi_0 \rangle\,, \tag{2}$$

where $\psi_\alpha(1)$ [$\psi^\dagger_\alpha(1)$] is an annihilation (creation) field operator of an electron with spin α and $\sigma^i_{\alpha\beta}$ are the elements of the Pauli spin matrices for $i = x, y, z$. The expectation value is taken with respect to the interacting many-body ground state $|\Psi_0\rangle$. For example, for the spin density in z direction, the operator is simply $\psi^\dagger_\uparrow(1)\psi_\uparrow(1) - \psi^\dagger_\downarrow(1)\psi_\downarrow(1)$, and the spin density is given by the difference of the spin-up and spin-down number densities. When considering transversal spin-wave excitations later on, the spin Pauli matrices for $i = x$ and $i = y$ will become relevant, but until then the derivation is general. The case $i = 0$ can be taken into account by defining $\sigma^0_{\alpha\beta} = \delta_{\alpha\beta}$. We rewrite Eq. (2) as

$$\sigma^i(1) = -\mathrm{i}\sum_{\alpha,\beta}\sigma^i_{\beta\alpha}G_{\alpha\beta}(11^+) \tag{3}$$

where $1^+ = \mathbf{r}_1 t_1 + \eta$ with a positive infinitesimal time η and $G_{\alpha\beta}(12) = -\mathrm{i}\langle\Psi_0|\mathscr{T}[\psi_\alpha(1)\psi^\dagger_\beta(2)]|\Psi_0\rangle$ is the interacting single-particle Green function with the time-ordering operator $\mathscr{T}$ (Mahan 2000), which orders the field operators chronologically from right to left. (A factor -1 has to be multiplied for each permutation of field operators.)

We are now in the position to prove that R^{ij} can be written as a spin-spin correlation function. First the Green function is expressed in the interaction picture

$$\begin{aligned} G_{\alpha\beta}(12) &= -\mathrm{i}\langle\Psi^{\mathrm{I}}_0(\infty)|U^{\mathrm{I}}(\infty,1)\psi^{\mathrm{I}}_\alpha(1)U^{\mathrm{I}}(1,2)\psi^{\mathrm{I}\dagger}_\beta(2)U^{\mathrm{I}}(2,-\infty)|\Psi_0\rangle \\ &= -\mathrm{i}\frac{\langle\Psi_0|U^{\mathrm{I}}(\infty,1)\psi^{\mathrm{I}}_\alpha(1)U^{\mathrm{I}}(1,2)\psi^{\mathrm{I}\dagger}_\beta(2)U^{\mathrm{I}}(2,-\infty)|\Psi_0\rangle}{\langle\Psi_0|U(\infty,-\infty)|\Psi_0\rangle}, \end{aligned} \tag{4}$$

where we have assumed that $t_1 > t_2$, that the Heisenberg state $|\Psi_0\rangle$ is identical to $|\Psi^{\mathrm{I}}_0(-\infty)\rangle$, and that $|\Psi^{\mathrm{I}}_0(\infty)\rangle$ differs from $|\Psi_0\rangle$ only by a phase factor. The time evolution operator depends only on the time arguments and fulfills the Tomonaga-Schwinger equation

$$\mathrm{i}\frac{\partial}{\partial t}U^{\mathrm{I}}(t,t') = H^{\mathrm{I}}(t)U^{\mathrm{I}}(t,t') \tag{5}$$

with the Zeeman term $H^{\mathrm{I}}(t') = \sum_{j,\alpha,\beta}\sigma^j_{\alpha\beta}\int B^j(1)\psi^{\mathrm{I}\dagger}_\alpha(1)\psi^{\mathrm{I}}_\beta(1)d1$. Using the solution $U^{\mathrm{I}}(t,t') = \mathscr{T}\exp\left[-\mathrm{i}\int_{t'}^{t} H^{\mathrm{I}}_j(t'')dt''\right]$, one can show that

$$\frac{\delta U^{\mathrm{I}}(t,t')}{\delta B^j(3)} = \begin{cases} -\mathrm{i}U^{\mathrm{I}}(t,t_3)\hat{\sigma}^j(3)U^{\mathrm{I}}(t_3,t') & \text{if } t < t_3 < t' \\ 0 & \text{otherwise} \end{cases} \tag{6}$$

with $\hat{\sigma}^j(3) = \sum_{\alpha,\beta}\sigma^j_{\alpha\beta}\psi^{\mathrm{I}\dagger}_\alpha(3)\psi^{\mathrm{I}}_\beta(3)$. This expression replaces the corresponding U^{I} when Eq. (4) is differentiated. Then, transforming back to the Heisenberg picture,

including the case $t_1 < t_2$, and inserting the result into Eqs. (1) and (3) yields the spin-spin correlation function

$$R^{ij}(12) = -\mathrm{i}\langle\Psi_0|\mathcal{T}[\hat{\sigma}^{i\prime}(1)\hat{\sigma}^{j\prime}(2)]|\Psi_0\rangle \tag{7}$$

with $\hat{\sigma}^{i\prime}(1) = \hat{\sigma}^{i}(1) - \sigma^{i}(1)$.

The reformulation with the Green function makes Eq. (3) amenable to a treatment within MBPT. The equation of motion of the Green function, the Dyson equation, in the presence of a $\mathbf{B}$ field reads

$$\left[\mathrm{i}\frac{\partial}{\partial t_1} + \frac{1}{2}\nabla^2_{\mathbf{r}_1} - V^{\mathrm{ext}}(\mathbf{r}_1)\right] G_{\alpha\beta}(12) - \left[\sum_i \sigma^i_{\alpha\beta} B^i(1)\right] G_{\alpha\beta}(12)$$
$$- \sum_\gamma \int M_{\alpha\gamma}(13) G_{\gamma\beta}(32) d3 = \delta(12)\delta_{\alpha\beta}\,, \tag{8}$$

from which we can directly identify the inverse of the Green function

$$G^{-1}_{\alpha\beta}(12) = \left[\mathrm{i}\frac{\partial}{\partial t_1} + \frac{1}{2}\nabla^2_{\mathbf{r}_1} - V^{\mathrm{ext}}(\mathbf{r}_1)\right]\delta(12)\delta_{\alpha\beta} - \left[\sum_i \sigma^i_{\alpha\beta} B^i(1)\right]\delta(12) - M_{\alpha\beta}(12) \tag{9}$$

with the external potential $V^{\mathrm{ext}}(\mathbf{r})$ and the delta function $\delta(12) = \delta(\mathbf{r}_1 - \mathbf{r}_2)\delta(t_1 - t_2)$. We have assumed the $\mathbf{B}$ field to incorporate a factor $g_{\mathrm{e}}\mu_{\mathrm{B}}/2$ ($g_{\mathrm{e}}/4$ in atomic units) with the electron spin g-factor g_{e} and the Bohr magneton μ_{B} so that $\mathbf{B}\cdot\hat{\sigma}$ is the Zeeman term of the Hamiltonian.

In solids, the orbital magnetic moment is usually strongly quenched, which is why we neglect the coupling of the $\mathbf{B}$ field to the orbital motion. The mass operator

$$M_{\alpha\beta}(12) = V^{\mathrm{H}}(1)\delta(12)\delta_{\alpha\beta} + \Sigma_{\alpha\beta}(12) \tag{10}$$

accounts for the electron-electron interaction. It embodies the Hartree potential

$$V^{\mathrm{H}}(1) = \int n(2) v(21) d2 = -\mathrm{i}\sum_\alpha \int G_{\alpha\alpha}(22^+) v(21) d2 \tag{11}$$

with the bare Coulomb interaction $v(12) = \delta(t_1 - t_2)/|\mathbf{r}_1 - \mathbf{r}_2|$ and the self-energy $\Sigma_{\alpha\beta}(12)$, a time-dependent nonlocal potential that incorporates all many-body exchange and correlation effects of the electronic system. The self-energy is the most complex quantity in Eq. (9), and its exact form is unknown. We employ the GW approximation (Hedin 1965)

$$\Sigma_{\alpha\beta}(12) = \mathrm{i} G_{\alpha\beta}(12) W(1^+2)\,, \tag{12}$$

where

$$W(12) = v(12) + \iint v(13)\,P(34)\,W(42)\,d3\,d4 \tag{13}$$

is the screened interaction, which is the effective potential at 1 created by a unit charge at 2 (first term) and the induced charge cloud forming around the unit charge (second term). The screened interaction is a dynamical (i.e., time-dependent) quantity, since the screening process requires the electrons to move, and this process takes time. Equation (13) is formally exact. The approximation consists in the choice of the polarization function, for which we use the RPA

$$P(12) = -\mathrm{i}\sum_{\alpha,\beta} G_{\alpha\beta}(12)G_{\beta\alpha}(21^{+})\,. \tag{14}$$

We note that Eq. (12) is defined with the self-consistently renormalized Green function, formally corresponding to a fully self-consistent solution of Hedin's equations (Hedin 1965) where the vertex function is approximated by $\Gamma(12;3) = \delta(12)\delta(13)$. This will become important in Sect. 4.

The derivative of G can be related to that of G^{-1} by differentiating both sides of $\sum_{\gamma} G_{\alpha\gamma}(13)G^{-1}_{\gamma\beta}(32)d3 = \delta(12)\delta_{\alpha\beta}$, yielding

$$\frac{\delta G_{\alpha\beta}(12)}{\delta B^{j}(3)} = -\sum_{\gamma,\delta}\iint G_{\alpha\gamma}(14)\frac{\delta G^{-1}_{\gamma\delta}(45)}{\delta B^{j}(3)}G_{\delta\beta}(52)d4\,d5\,. \tag{15}$$

Through the derivative of Eq. (9)

$$\frac{\delta G^{-1}_{\alpha\beta}(12)}{\delta B^{j}(3)} = -\sigma^{j}_{\alpha\beta}\delta(13)\delta(12) - \frac{\delta M_{\alpha\beta}(12)}{\delta B^{j}(3)} \tag{16}$$

and Eqs. (10), (11), and (12), the right-hand side of Eq. (15) can be expressed in terms of $\delta G/\delta B$, and successive insertion will lead to an infinite series expansion. Before we do this step, we have to find a suitable expression for the second term of $\delta\Sigma/\delta B = \mathrm{i}(\delta G/\delta B)W + \mathrm{i}G(\delta W/\delta B)$. Differentiating Eq. (13), solving for the derivative of W, and using Eq. (14) gives

$$\begin{aligned}\frac{\delta W(12)}{\delta B^{j}(3)} &= -\mathrm{i}\sum_{\alpha,\beta}\iint W(14)\\ &\quad\left[\frac{\delta G_{\alpha\beta}(45)}{\delta B^{j}(3)}G_{\beta\alpha}(54^{+}) + G_{\alpha\beta}(45)\frac{\delta G_{\beta\alpha}(54^{+})}{\delta B^{j}(3)}\right]W(52)\,d4\,d5\,.\end{aligned} \tag{17}$$

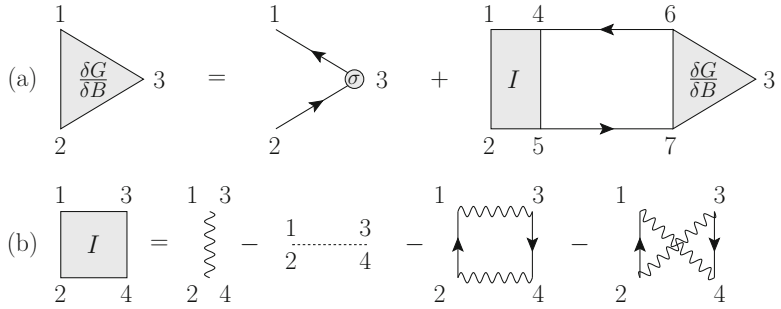

Fig. 1 Diagrammatic representations of (**a**) Eq. (18) and (**b**) Eq. (19). Successive reinsertion in (**a**) produces an infinite series of diagrams for $\delta G/\delta B$ and, hence, for R. Arrows represent the renormalized Green function, the dotted line the bare, and the wiggly line the screened interaction. (We use the convention that each interaction line carries a factor i.) The spin-flip operator, mathematically described by a Pauli matrix, is shown as σ

Now, we can combine everything and obtain

$$\frac{\delta G_{\alpha\beta}(12)}{\delta B^j(3)} = \sum_{\gamma,\delta}\Bigg[\sigma^j_{\gamma\delta} G_{\alpha\gamma}(13) G_{\delta\beta}(32^+) + \sum_{\varepsilon,\zeta}\iiiint G_{\alpha\gamma}(14) G_{\delta\beta}(52^+) I_{\gamma\delta,\varepsilon\zeta}(45,67)\frac{\delta G_{\varepsilon\zeta}(67)}{\delta B^j(3)} d4\, d5\, d6\, d7\Bigg] \tag{18}$$

with the (irreducible) interaction kernel

$$I_{\alpha\beta,\gamma\delta}(12,34) = \mathrm{i}\big[W(1^+2)\delta(13)\delta(24)\delta_{\alpha\gamma}\delta_{\beta\delta} - v(13)\delta_{\alpha\beta}\delta_{\gamma\delta}\delta(12)\delta(3^+4)\big] + G_{\alpha\beta}(12)\big[W(1^+3)G_{\delta\gamma}(43^+)W(42) + W(1^+4)G_{\delta\gamma}(43^+)W(32)\big]. \tag{19}$$

Equation (18) defines an infinite series expansion for $\delta G/\delta B$ as shown diagrammatically in Fig. 1a. By virtue of the Eqs. (1) and (3), a corresponding series expansion is obtained for $R^{ij}(12)$.

For $i = j = 0$, the above formulas lead to the Bethe-Salpeter equation for optical absorption. The case $i = 0 \neq j$ (or vice versa) describes the coupling of electronic spin and charge. The equations simplify in the absence of spin-orbit coupling. The Green function is then diagonal in spin space, and the inner spin summations in Eq. (18) disappear. We now discuss some specific cases:

Nonmagnetic case: We have $G_{\alpha\beta}(12) = \delta_{\alpha\beta} G(12)$, i.e., spin-up and spin-down Green functions are identical. As a result, all degrees of freedom (0, x, y, and z) decouple and $R^{00} = R^{zz}$ and $R^{xx} = R^{yy}$.

Collinear (anti-)ferromagnetism: The Green function is still diagonal in spin space, but the two components are different, i.e., $G_{\alpha\beta}(12) = \delta_{\alpha\beta} G_\alpha(12)$. Then, the degrees of freedom 0 and z as well as x and y couple. In particular, we get a coupling of the spin and charge degrees of freedom in R^{0z} (and R^{z0}). The diagonal elements R^{00} and R^{zz} are the density response function and the longitudinal spin susceptibility, respectively. They are decoupled from the functions R^{ij} with $i, j \in \{x, y\}$, which give rise to the transverse spin susceptibility. In the latter case, the interaction kernel reduces to the first term $I = \mathrm{i}W$.

Spin-orbit coupling: In the presence of spin-orbit coupling, the Green function acquires spin-off-diagonal elements. Then all degrees of freedom couple in general and all terms in Eq. (19) and all response functions defined in Eq. (1) must be taken into account.

In the following, we restrict ourselves to the case of spin excitations in a ferromagnet with a collinear magnetic ground state without spin-orbit coupling. For a spin polarization along the z axis, these are generated by an oscillating magnetic field in the xy plane. In particular, in inelastic neutron scattering experiments, the incoming neutron beam is circularly polarized, creating a magnetic field whose y component exhibits a phase shift of $\pi/2$ with respect to the x component (Lowde et al. 1983).

It is instructive to discuss the coupling of the electron's spin to the **B** field in terms of semiclassical physics. Without the perturbing field, the electron spin **S** precesses around the Weiss (exchange) field $\mathbf{B}_0$ according to the equation of motion $\dot{\mathbf{S}} = \boldsymbol{\mu} \times \mathbf{B}_0$, where $\boldsymbol{\mu} = -g_\mathrm{e}\mu_\mathrm{B}\mathbf{S}/\hbar$ is the magnetic moment of the electron. (We write the formulas in SI units in this paragraph.) With the majority spin pointing in the positive **z** direction, the Weiss field points in the negative **z** direction, and $\boldsymbol{\omega}_0 = g_\mathrm{e}\mu_\mathrm{B}\mathbf{B}_0/\hbar$ is the Larmor frequency of the precession. The two possible circular polarizations of the perturbing **B** field – right- and left-handed with respect to the $\mathbf{B}_0$ field – are given by $\mathbf{B}^\pm(t) = B^\pm \mathrm{Re}[(\hat{\mathbf{x}} \mp \mathrm{i}\hat{\mathbf{y}})e^{-\mathrm{i}\omega t}]$, respectively. The equation of motion in the presence of the perturbing field is $\dot{\mathbf{S}} = \boldsymbol{\mu} \times (\mathbf{B}_0 + \mathbf{B}^\pm)$. If $\mathbf{S}^\pm$ is defined as the spin vector seen in the coordinate system that rotates with the $\mathbf{B}^\pm$ field, we can write $\dot{\mathbf{S}} = \dot{\mathbf{S}}^\pm - \mathbf{S} \times \boldsymbol{\omega}$. Equating the right-hand sides of the last two equations and inserting the formulas for $\boldsymbol{\mu}$ and $\boldsymbol{\omega}_0$ gives $\dot{\mathbf{S}}^\pm = \boldsymbol{\mu} \times \mathbf{B}^\pm + \mathbf{S} \times (\boldsymbol{\omega} - \boldsymbol{\omega}_0)$, which reduces to $\dot{\mathbf{S}}^\pm = \boldsymbol{\mu} \times \mathbf{B}^\pm$ if $\boldsymbol{\omega}$=$\boldsymbol{\omega}_0$. This is the equation of motion of a spin precessing around $\mathbf{B}^\pm$, i.e., around a direction perpendicular to $\mathbf{B}_0$, making it possible to flip the spin of the electron. The frequency of this precession, the Rabi frequency, is $g_\mathrm{e}\mu_\mathrm{B}B/\hbar$. The condition that $\boldsymbol{\omega}$ and $\boldsymbol{\omega}_0 = g_\mathrm{e}\mu_\mathrm{B}\mathbf{B}_0/\hbar$ have the same orientation is fulfilled for the right-handed circular polarization, for which the relevant component is $B^+ = B_x + \mathrm{i}B_y$ because $B_x\hat{\mathbf{x}} + B_y\hat{\mathbf{y}} = B^+(\hat{\mathbf{x}} - \mathrm{i}\hat{\mathbf{y}}) + B^-(\hat{\mathbf{x}} + \mathrm{i}\hat{\mathbf{y}})$ with $B^- = B_x - \mathrm{i}B_y$.

Therefore, we consider the transverse magnetic susceptibility

$$R^{+-}(12) = \frac{\delta\sigma^+(1)}{\delta B^+(2)} \tag{20}$$

in the following, where "+" and "−" refer to the Pauli matrices $\hat{\sigma}^+ = \hat{\sigma}^x + \mathrm{i}\hat{\sigma}^y$ and $\hat{\sigma}^- = \hat{\sigma}^x - \mathrm{i}\hat{\sigma}^y$ with the matrix representations

$$\sigma^+ = \begin{pmatrix} 0 & 2 \\ 0 & 0 \end{pmatrix} \quad \text{and} \quad \sigma^- = \begin{pmatrix} 0 & 0 \\ 2 & 0 \end{pmatrix} \tag{21}$$

for the spin creation and annihilation operators. The Zeeman term of Eq. (9) can be written as

$$\sum_i \sigma^i_{\alpha\beta} B^i(1) = \frac{1}{2}\left[\sigma^+_{\alpha\beta} B^-(1) + \sigma^-_{\alpha\beta} B^+(1)\right] + \sigma^z_{\alpha\beta} B^z(1). \tag{22}$$

Because of the mixed products of the form $\sigma^+ B^-$ and $\sigma^- B^+$, the spin-spin correlation function Eq. (7) becomes

$$R^{+-}(12) = \frac{\delta\sigma^+(1)}{\delta B^+(2)} = -\mathrm{i}\langle\Psi_0|\mathscr{T}[\hat{\sigma}^+(1)\hat{\sigma}^-(2)]|\Psi_0\rangle\,, \tag{23}$$

where we have used that $\langle\Psi_0|\hat{\sigma}^+(1)|\Psi_0\rangle = \langle\Psi_0|\hat{\sigma}^-(1)|\Psi_0\rangle = 0$ in a collinear magnetic system. This form of the spin-spin correlation function is intuitive: for a spin in the up channel to be probed, one has to flip its spin with the operator $\hat{\sigma}^-$ before flipping it back with $\hat{\sigma}^+$. Equation (23) also explains the notation R^{+-}.

With Eq. (22), a derivation that proceeds in analogy to above leads to

$$\mathrm{i}\frac{\delta G_{\downarrow\uparrow}(12)}{\delta B^+(3)} = K_{\downarrow\uparrow}(12,33) + \iint K_{\downarrow\uparrow}(12,45) W(4^+5) \mathrm{i}\frac{\delta G_{\downarrow\uparrow}(45)}{\delta B^j(3)} d4\, d5 \tag{24}$$

with the (uncorrelated) two-particle propagator

$$K_{\downarrow\uparrow}(12,34) = \mathrm{i} G_\downarrow(13) G_\uparrow(42^+) \tag{25}$$

($G_\uparrow = G_{\uparrow\uparrow}$, $G_\downarrow = G_{\downarrow\downarrow}$). We have used that (a) the mass operator Eq. (10) reduces to Σ for $\alpha \neq \beta$ and (b) the second term in Eq. (19) vanishes, (c) as do the last two terms because the Green function is diagonal in spin space. Note that Eq. (24) can be obtained from Eq. (18) by setting $i = +$ and $j = -$ except for an additional factor 1/2 from Eq. (22).

Equation (24) can be written as a matrix equation if we define a generalized four-point magnetic response function (formally giving the response of the spin density matrix with respect to changes of a nonlocal **B** field). To this end, we introduce

the auxiliary four-point magnetic response function defined by the Bethe-Salpeter equation

$$R^{(4)}_{\downarrow\uparrow}(12,34) = K_{\downarrow\uparrow}(12,34) + \iint K_{\downarrow\uparrow}(12,56)W(5^+6)R^{(4)}_{\downarrow\uparrow}(56,34)d5\,d6\,, \tag{26}$$

from which we deduce

$$R^{(4)}_{\downarrow\uparrow}(12,33) = \mathrm{i}\frac{\delta G_{\downarrow\uparrow}(12)}{\delta B^+(3)} \tag{27}$$

$$R^{+-}(12) = -2R^{(4)}_{\downarrow\uparrow}(11,22)\,. \tag{28}$$

The magnetic response function can, furthermore, be written as the sum of two terms

$$R^{+-}(12) = -2K_{\downarrow\uparrow}(11,22) - 2\iiiint K_{\downarrow\uparrow}(11,34)T_{\downarrow\uparrow}(34,56) K_{\downarrow\uparrow}(56,22)d3\,d4\,d5\,d6\,, \tag{29}$$

where the T matrix, which can be interpreted as a reducible interaction kernel, fulfills the equation

$$T_{\downarrow\uparrow}(12,34) = W(1^+2)\delta(13)\delta(24) + \iint W(1^+2)K_{\downarrow\uparrow}(12,56)T_{\downarrow\uparrow}(56,34)d5\,d6\,. \tag{30}$$

If we approximate the renormalized Green function in Eq. (25) by the Kohn-Sham Green function, then the first term of Eq. (29) contains single-particle excitations between Kohn-Sham levels from one spin channel into the other. The second term describes the correlated motion of an electron-hole pair with opposite spins through the T matrix Fig. 2; each ladder diagram stands for a series of scattering events. This correlated motion is responsible for the occurrence of collective spin excitations. The second term also renormalizes the Stoner excitations.

TDDFT (Runge and Gross 1984) is another method that allows one to calculate the magnetic response function from first principles. In this theory, Eq. (3) is written in terms of the Kohn-Sham Green function $G^{\mathrm{KS}}_{\alpha\beta}(12)$ instead of $G_{\alpha\beta}(12)$. This

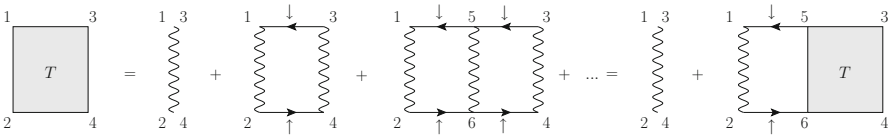

Fig. 2 Diagrammatic representation of the $T_{\downarrow\uparrow}(12,34)$ matrix consisting of an infinite series of ladder diagrams, each wiggly line (screened interaction W) representing a "rung" of the ladder. The indices 5 and 6 denote integration variables

is not an approximation since the Kohn-Sham system (Kohn and Sham 1965) is constructed to yield the *exact* electronic spin density of the interacting system (provided that the exact exchange-correlation functional is employed). A derivation, similar to the one above with Σ in Eq. (10) replaced by the exchange-correlation potential $v^{\mathrm{xc}}_{\alpha\beta}(1)$, then yields an expression for the magnetic response function with the interaction kernel

$$I^{\mathrm{KS}}_{\alpha\beta,\gamma\delta}(12,34) = -\mathrm{i}\left[v(13)\delta_{\alpha\beta}\delta_{\gamma\delta} + f^{\mathrm{xc}}_{\alpha\beta,\gamma\delta}(13)\right]\delta(12)\delta(3^{+}4)\,, \tag{31}$$

where $f^{\mathrm{xc}}_{\alpha\beta,\gamma\delta}(12) = \delta v^{\mathrm{xc}}_{\alpha\beta}(1)/\delta\sigma_{\gamma\delta}(2)$ is the exchange-correlation kernel of TDDFT. This interaction kernel is effectively just a two-point function. Equation (26), hence, turns into a two-point matrix equation, which makes the implementation of the TDDFT approach much simpler and computationally less demanding. However, there are only few approximations available for $f^{\mathrm{xc}}_{\alpha\beta,\gamma\delta}(12)$ to date, which, at that, cannot be systematically improved in contrast to the electronic self-energy. The most common approximation, the adiabatic local-density approximation, neglects time dependence and nonlocality altogether (and also requires the spin indices to be pairwise identical) so that $f^{\mathrm{xc}}_{\alpha\beta,\beta\alpha}(1)$ becomes a local function. Still, several publications (Savrasov 1998; Buczek et al. 2009, 2010, 2011; Lounis et al. 2010, 2011) have demonstrated that the spin excitation spectra calculated within TDDFT are often in good agreement to results from MBPT and to experiment.

3 Implementation

In this section, we present the basics of a numerical implementation in the SPEX code (Friedrich et al. 2010). For more details, we refer the reader to Friedrich et al. (2014). The four-point quantities derived in the previous section are represented in a basis of Wannier functions. In Sect. 4, we will discuss and compare several mean-field systems as the reference noninteracting system. In the present section, we assume the Kohn-Sham solution (Kohn and Sham 1965) of density functional theory (DFT) (Hohenberg and Kohn 1964) be used. The corresponding Kohn-Sham equations are solved within the all-electron FLAPW method as implemented in the FLEUR code (http://www.flapw.de), which allows an accurate representation of the single-particle states $\varphi^{\alpha}_{\mathbf{k}m}(\mathbf{r})$, where $\mathbf{k}$ is the Bloch vector and m the band index.

For a practical implementation, Eq. (26) is too complex because it contains quantities that, in general, depend on four points in space and on four time (or frequency) arguments (three if the Hamiltonian is time independent). A first simplification uses the fact that the spin-wave excitations are usually of low frequency, which motivates to replace the screened interaction by its static limit, i.e., $W(\mathbf{r}_1,\mathbf{r}_2;\omega) \to W(\mathbf{r}_1,\mathbf{r}_2;0) = W(\mathbf{r}_1,\mathbf{r}_2)$, implying an instantaneous interaction in time, $W(\mathbf{r}_1 t_1,\mathbf{r}_2 t_2) = W(\mathbf{r}_1,\mathbf{r}_2)\delta(t_1 - t_2)$. For example, the two-particle propagator Eq. (25) then only depends on a single time (or frequency) argument because the delta function in the previous expression (and the contraction of

Eq. (28)) requires the argument pairs 12 and 34 to have the same time argument, i.e., $K_{\downarrow\uparrow}(\mathbf{r}_1, \mathbf{r}_2; \mathbf{r}_3, \mathbf{r}_4; \tau = t_1 - t_3)$ with $t_1 = t_2$ and $t_3 = t_4$. Equation (26) then simplifies to

$$R^{(4)}_{\downarrow\uparrow}(\mathbf{r}_1, \mathbf{r}_2; \mathbf{r}_3, \mathbf{r}_4; \omega) = K_{\downarrow\uparrow}(\mathbf{r}_1, \mathbf{r}_2; \mathbf{r}_3, \mathbf{r}_4; \omega) + \iint K_{\downarrow\uparrow}(\mathbf{r}_1, \mathbf{r}_2; \mathbf{r}_5, \mathbf{r}_6; \omega) W(\mathbf{r}_5, \mathbf{r}_6) R^{(4)}_{\downarrow\uparrow}(\mathbf{r}_5, \mathbf{r}_6; \mathbf{r}_3, \mathbf{r}_4; \omega)\, d^3r_5\, d^3r_6 \tag{32}$$

in the frequency domain. We employ another approximation in that we allow electrons (and holes) to interact with each other only when they are located on the same atomic site, thus making use of the fact that the screened interaction is short range in metallic systems. This on-site approximation is not strictly necessary, but it greatly simplifies the implementation and enables fast calculations. Besides, it is a very good approximation for the systems studied here (Müller et al. 2016).

Wannier functions (Marzari and Vanderbilt 1997) are localized functions defined by linear combinations of the single-particle wave functions

$$w^{\alpha}_{\mathbf{R}n}(\mathbf{r}) = \frac{1}{N} \sum_{\mathbf{k}} e^{-\mathrm{i}\mathbf{k}\cdot\mathbf{R}} \sum_{m} U^{\alpha}_{\mathbf{k}m,n} \varphi^{\alpha}_{\mathbf{k}m}(\mathbf{r})\,, \tag{33}$$

where n is an index counting the Wannier functions at the atomic site $\mathbf{R}$ and N is the number of $\mathbf{k}$ points of an $N_x \times N_y \times N_z$ Monkhorst-Pack set (Monkhorst and Pack 1976) including $\mathbf{k} = \mathbf{0}$. The transformation matrix $U^{\alpha}_{\mathbf{k}m,n}$ is determined by minimizing the spread of the Wannier functions (Souza et al. 2001; Marzari and Vanderbilt 1997; Freimuth et al. 2008), under the condition that the Wannier functions are orthonormal with respect to integrations over the $N_x \times N_y \times N_z$ supercell (whereas the $\varphi^{\alpha}_{\mathbf{k}m}(\mathbf{r})$ are orthonormalized with respect to the unit cell). The sum over m runs over a limited number of electronic bands (at least as many as the number of Wannier functions).

In the frequency domain, Eq. (25) becomes

$$\begin{aligned} K_{\downarrow\uparrow}(\mathbf{r}_1, \mathbf{r}_2; \mathbf{r}_3, \mathbf{r}_4; \omega) &= \frac{\mathrm{i}}{2\pi} \int_{-\infty}^{\infty} G_{\downarrow}(\mathbf{r}_1, \mathbf{r}_3; \omega') G_{\uparrow}(\mathbf{r}_4, \mathbf{r}_2; \omega' - \omega) d\omega' \\ &= \frac{1}{N^2} \sum_{\mathbf{k}} \sum_{\mathbf{k}'} \sum_{m}^{\text{occ.}} \sum_{m'}^{\text{unocc.}} \left\{ \frac{\varphi^{\downarrow}_{\mathbf{k}m}(\mathbf{r}_1) \varphi^{\downarrow *}_{\mathbf{k}m}(\mathbf{r}_3) \varphi^{\uparrow *}_{\mathbf{k}'m'}(\mathbf{r}_2) \varphi^{\uparrow}_{\mathbf{k}'m'}(\mathbf{r}_4)}{\omega + \varepsilon^{\uparrow}_{\mathbf{k}'m'} - \varepsilon^{\downarrow}_{\mathbf{k}m} - \mathrm{i}\eta} \right. \\ &\quad \left. - \frac{\varphi^{\downarrow}_{\mathbf{k}'m'}(\mathbf{r}_1) \varphi^{\downarrow *}_{\mathbf{k}'m'}(\mathbf{r}_3) \varphi^{\uparrow *}_{\mathbf{k}m}(\mathbf{r}_2) \varphi^{\uparrow}_{\mathbf{k}m}(\mathbf{r}_4)}{\omega + \varepsilon^{\uparrow}_{\mathbf{k}m} - \varepsilon^{\downarrow}_{\mathbf{k}'m'} + \mathrm{i}\eta} \right\} \end{aligned} \tag{34}$$

with a positive infinitesimal η, where we have used the Lehmann representation of the noninteracting Kohn-Sham Green function

$$G_\alpha(\mathbf{r},\mathbf{r}';\omega)=\frac{1}{N}\sum_{\mathbf{k}}\sum_{m}\frac{\varphi^{\alpha}_{\mathbf{k}m}(\mathbf{r})\varphi^{\alpha *}_{\mathbf{k}m}(\mathbf{r}')}{\omega-\varepsilon^{\alpha}_{\mathbf{k}m}+\mathrm{i}\eta\,\mathrm{sgn}(\varepsilon^{\alpha}_{\mathbf{k}m}-\varepsilon_{\mathrm{F}})} \tag{35}$$

with the Fermi energy ε_{F}.

Each of the four vertices of $K_{\downarrow\uparrow}(\mathbf{r}_1,\mathbf{r}_2;\mathbf{r}_3,\mathbf{r}_4;\omega)$ is now projected onto the Wannier basis defined by Eq. (33), which gives

$$\begin{aligned}K^{\downarrow\uparrow}_{\mathbf{R}n_1\mathbf{R}n_2,\mathbf{R}'n_3\mathbf{R}'n_4}(\omega)=\frac{1}{N^2}\sum_{\mathbf{k}m}^{\text{occ.}}\sum_{\mathbf{k}'m'}^{\text{unocc.}}\Bigg\{&\frac{U^{\downarrow *}_{\mathbf{k}m,n_1}U^{\downarrow}_{\mathbf{k}m,n_3}U^{\uparrow}_{\mathbf{k}'m',n_2}U^{\uparrow *}_{\mathbf{k}'m',n_4}}{\omega+\varepsilon^{\uparrow}_{\mathbf{k}'m'}-\varepsilon^{\downarrow}_{\mathbf{k}m}-\mathrm{i}\eta}e^{-\mathrm{i}(\mathbf{k}'-\mathbf{k})(\mathbf{R}-\mathbf{R}')}\\&-\frac{U^{\downarrow *}_{\mathbf{k}'m',n_1}U^{\downarrow}_{\mathbf{k}'m',n_3}U^{\uparrow}_{\mathbf{k}m,n_2}U^{\uparrow *}_{\mathbf{k}m,n_4}}{\omega+\varepsilon^{\uparrow}_{\mathbf{k}m}-\varepsilon^{\downarrow}_{\mathbf{k}'m'}+\mathrm{i}\eta}e^{\mathrm{i}(\mathbf{k}'-\mathbf{k})(\mathbf{R}-\mathbf{R}')}\Bigg\},\end{aligned} \tag{36}$$

where the on-site approximation has been used to set $\mathbf{R}_1=\mathbf{R}_2=\mathbf{R}$ and $\mathbf{R}_3=\mathbf{R}_4=\mathbf{R}'$. This expression only depends on $\Delta\mathbf{R}=\mathbf{R}-\mathbf{R}'$, and a lattice Fourier transformation yields

$$\begin{aligned}K^{\downarrow\uparrow}_{n_1n_2,n_3n_4}(\mathbf{q},\omega)&=\sum_{\Delta\mathbf{R}}K^{\downarrow\uparrow}_{\mathbf{R}n_1\mathbf{R}n_2,\mathbf{R}-\Delta\mathbf{R}n_3\mathbf{R}-\Delta\mathbf{R}n_4}(\omega)e^{-\mathrm{i}\mathbf{q}\cdot\Delta\mathbf{R}}\\&=\frac{1}{N}\sum_{\mathbf{k}}\sum_{m}^{\text{occ.}}\sum_{m'}^{\text{unocc.}}\Bigg\{\frac{U^{\downarrow *}_{\mathbf{q}+\mathbf{k}m,n_1}U^{\downarrow}_{\mathbf{q}+\mathbf{k}m,n_3}U^{\uparrow}_{\mathbf{k}m',n_2}U^{\uparrow *}_{\mathbf{k}m',n_4}}{\omega+\varepsilon^{\uparrow}_{\mathbf{k}m'}-\varepsilon^{\downarrow}_{\mathbf{q}+\mathbf{k}m}-\mathrm{i}\eta}\\&\quad-\frac{U^{\downarrow *}_{\mathbf{q}+\mathbf{k}m',n_1}U^{\downarrow}_{\mathbf{q}+\mathbf{k}m',n_3}U^{\uparrow}_{\mathbf{k}m,n_2}U^{\uparrow *}_{\mathbf{k}m,n_4}}{\omega+\varepsilon^{\uparrow}_{\mathbf{k}m}-\varepsilon^{\downarrow}_{\mathbf{q}+\mathbf{k}m'}+\mathrm{i}\eta}\Bigg\}.\end{aligned} \tag{37}$$

We use the tetrahedron method (Rath and Freeman 1975) for the $\mathbf{k}$ summation.

From this equation, it is clear that if $\mathbf{q}$ and $\mathbf{k}$ are elements of the $\mathbf{k}$-point set, then $\mathbf{q}+\mathbf{k}$ must be an element of the set, too. The Monkhorst-Pack grid fulfills this condition. On the other hand, this condition limits the number of $\mathbf{q}$ points at which a spin excitation spectrum can be calculated to the relatively few points of the $\mathbf{k}$-point set. In order to evaluate K (and R) at an arbitrary Bloch vector $\mathbf{q}$, which would enable the calculation of smooth spin-wave dispersion curves, we have to introduce an auxiliary set of Wannier functions with a suitable Bloch character

$$\tilde{w}^{\alpha}_{\mathbf{R}n}(\mathbf{r})=\frac{1}{N}\sum_{\mathbf{k}}e^{-\mathrm{i}(\mathbf{k}+\mathbf{q})\cdot\mathbf{R}}\sum_{m}U^{\alpha}_{\mathbf{k}+\mathbf{q}m,n}\varphi^{\alpha}_{\mathbf{k}+\mathbf{q}m}(\mathbf{r})\,, \tag{38}$$

where the transformation matrices are distinguished from the ones used in Eq. (33) by the Bloch vectors $\mathbf{k}+\mathbf{q}$, which are generally not elements of the original $\mathbf{k}$-point set. With this definition, Eq. (37) remains valid, but it has to be taken into account

that the transformation matrices $U^{\alpha}_{\mathbf{q}+\mathbf{k}m,n}$ and $U^{\alpha}_{\mathbf{k}m,n}$ now belong to two different sets of Wannier functions.

The second quantity that we need for solving Eq. (26) is the screened interaction. We define its Wannier representation by

$$W^{\downarrow\uparrow}_{\mathbf{R}n_1\mathbf{R}n_2,\mathbf{R}n_3\mathbf{R}n_4}(\omega)=\frac{N}{\mathcal{N}}\iint w^{\downarrow *}_{\mathbf{R}n_1}(\mathbf{r})w^{\downarrow}_{\mathbf{R}n_3}(\mathbf{r})W(\mathbf{r},\mathbf{r}';\omega)w^{\uparrow}_{\mathbf{R}n_2}(\mathbf{r}')w^{\uparrow *}_{\mathbf{R}n_4}(\mathbf{r}')d^3r\,d^3r'\,, \tag{39}$$

where $\mathcal{N}(\mathcal{N}/N)$ is the infinite number of unit cells (supercells). The prefactor is required to avoid double counting because the integrations extend over the whole infinite space. Inserting Eq. (33) gives

$$\begin{aligned} W^{\downarrow\uparrow}_{\mathbf{R}n_1\mathbf{R}n_2,\mathbf{R}n_3\mathbf{R}n_4}(\omega) = \frac{1}{N^3}\sum_{\mathbf{k},\mathbf{k}',\mathbf{k}''}\sum_{m_1,m_2,m_3,m_4} & U^{\downarrow *}_{\mathbf{k}+\mathbf{k}''m_1,n_1}U^{\downarrow}_{\mathbf{k}m_3,n_3}U^{\uparrow}_{\mathbf{k}'+\mathbf{k}''m_2,n_2}U^{\uparrow *}_{\mathbf{k}'m_4,n_4} \\ \times\frac{1}{\mathcal{N}}\iint & \varphi^{\downarrow *}_{\mathbf{k}+\mathbf{k}''m_1}(\mathbf{r})\varphi^{\downarrow}_{\mathbf{k}m_3}(\mathbf{r})W(\mathbf{r},\mathbf{r}';\omega)\varphi^{\uparrow}_{\mathbf{k}'+\mathbf{k}''m_2}(\mathbf{r}') \\ & \varphi^{\uparrow *}_{\mathbf{k}'m_4}(\mathbf{r}')d^3r\,d^3r'\,, \end{aligned} \tag{40}$$

where it has been used that $W(\mathbf{r},\mathbf{r}';\omega)$ is diagonal in $\mathbf{k}$. The evaluation of the double integral, which, together with the prefactor $1/\mathcal{N}$, is finite, is discussed elsewhere (Friedrich et al. 2009). Since Eq. (40) is independent of $\mathbf{R}$, we may write $W^{\downarrow\uparrow}_{n_1n_2,n_3n_4}(\omega)$.

We are now in the position to formulate the Bethe-Salpeter equation (Eq. (32)) in the Wannier basis

$$\begin{aligned} R^{(4)\downarrow\uparrow}_{\mathbf{R}n_1\mathbf{R}n_2,\mathbf{R}'n_3\mathbf{R}'n_4}(\omega) = K^{\downarrow\uparrow}_{\mathbf{R}n_1\mathbf{R}n_2,\mathbf{R}'n_3\mathbf{R}'n_4}(\omega) + \sum_{\mathbf{R}''}\sum_{n_5,n_6,n_7,n_8} & K^{\downarrow\uparrow}_{\mathbf{R}n_1\mathbf{R}n_2,\mathbf{R}''n_5\mathbf{R}''n_6}(\omega) \\ \times W^{\downarrow\uparrow}_{n_5n_6,n_7n_8}(0)R^{(4)\downarrow\uparrow}_{\mathbf{R}''n_7\mathbf{R}''n_8,\mathbf{R}'n_3\mathbf{R}'n_4}(\omega)\,. & \end{aligned} \tag{41}$$

As K (and hence also R) depends only on the difference $\Delta\mathbf{R} = \mathbf{R} - \mathbf{R}'$, we can insert the lattice Fourier transformations

$$K^{\downarrow\uparrow}_{\mathbf{R}n_1\mathbf{R}n_2,\mathbf{R}'n_3\mathbf{R}'n_4}(\omega) = \frac{1}{N}\sum_{\mathbf{q}} e^{\mathrm{i}\mathbf{q}\cdot(\mathbf{R}-\mathbf{R}')}K^{\downarrow\uparrow}_{n_1n_2,n_3n_4}(\mathbf{q},\omega)\,, \tag{42}$$

analogously for $R^{(4)}$, and obtain

$$\begin{aligned} R^{(4)\downarrow\uparrow}_{n_1n_2,n_3n_4}(\mathbf{q},\omega) = K^{\downarrow\uparrow}_{n_1n_2,n_3n_4}(\mathbf{q},\omega) + \sum_{n_5,n_6,n_7,n_8} & K^{\downarrow\uparrow}_{n_1n_2,n_5n_6}(\mathbf{q},\omega) \\ \times W^{\downarrow\uparrow}_{n_5n_6,n_7n_8}(0)R^{(4)\downarrow\uparrow}_{n_7n_8,n_3n_4}(\mathbf{q},\omega)\,. & \end{aligned} \tag{43}$$

This is a matrix equation in pairs of Wannier indices. Since Wannier functions are orthonormal, their pairs are orthonormal, too. The summations on the right-hand side are mere matrix multiplications, and we can formally solve Eq. (43) for $R^{(4)}$

$$R^{(4)\downarrow\uparrow}(\mathbf{q},\omega) = [\mathbb{1} - K^{\downarrow\uparrow}(\mathbf{q},\omega)W^{\downarrow\uparrow}(0)]^{-1}K^{\downarrow\uparrow}(\mathbf{q},\omega)\,. \tag{44}$$

Using Eq. (28), we obtain the physically relevant magnetic response function from the matrix elements of $R^{(4)\downarrow\uparrow}(\mathbf{q},\omega)$ by

$$R^{+-}(\mathbf{r},\mathbf{r}';\omega) = -\frac{2}{N}\sum_{\mathbf{q}}\sum_{n_1,n_2,n_3,n_4} R^{(4)\downarrow\uparrow}_{n_1n_2,n_3n_4}(\mathbf{q},\omega)\Omega^{\downarrow\uparrow}_{\mathbf{q}n_1n_2}(\mathbf{r})\Omega^{\downarrow\uparrow *}_{\mathbf{q}n_3n_4}(\mathbf{r}')\,. \tag{45}$$

where $\Omega^{\downarrow\uparrow}_{\mathbf{q}n_1n_2}(\mathbf{r})$ are the lattice Fourier transforms of the Wannier products $\Omega^{\alpha\beta}_{\mathbf{R},n_1n_2}(\mathbf{r}) = w^{\alpha}_{\mathbf{R}n_1}(\mathbf{r})w^{\beta *}_{\mathbf{R}n_2}(\mathbf{r})$, i.e.,

$$\Omega^{\alpha\beta}_{\mathbf{q}n_1n_2}(\mathbf{r}) = \sum_{\mathbf{R}}\Omega^{\alpha\beta}_{\mathbf{R}n_1n_2}(\mathbf{r})e^{\mathrm{i}\mathbf{q}\cdot\mathbf{R}} = \frac{1}{N}\sum_{\mathbf{k}} w^{\alpha}_{\mathbf{q}+\mathbf{k}n_1}(\mathbf{r})w^{\beta *}_{\mathbf{k}n_2}(\mathbf{r}) \tag{46}$$

with the Wannier Bloch functions $w^{\alpha}_{\mathbf{k}n}(\mathbf{r}) = \sum_m U^{\alpha}_{\mathbf{k}m,n}\varphi^{\alpha}_{\mathbf{k}m}(\mathbf{r})$. If we use the matrix representation of $K^{\downarrow\uparrow}(\mathbf{q},\omega)$ in Eq. (45), we obtain the bare susceptibility, i.e., the fictitious magnetic response function of the noninteracting reference system:

$$K^{+-}(\mathbf{r},\mathbf{r}';\omega) = -2K^{\downarrow\uparrow}(\mathbf{r},\mathbf{r};\mathbf{r}',\mathbf{r}';\omega) \tag{47}$$

$$= -\frac{2}{N}\sum_{\mathbf{q}}\sum_{n_1,n_2,n_3,n_4} K^{\downarrow\uparrow}_{n_1n_2,n_3n_4}(\mathbf{q},\omega)\Omega^{\downarrow\uparrow}_{\mathbf{q}n_1n_2}(\mathbf{r})\Omega^{\downarrow\uparrow *}_{\mathbf{q}n_3n_4}(\mathbf{r}')\,. \tag{48}$$

Of course, $R^{+-}(\mathbf{r},\mathbf{r}';\omega)$ is still a very complex quantity: it is nonlocal in space, it shows a frequency dependence, and it has a real and an imaginary part. The spectrum measured in neutron scattering experiments, for example, can be extracted from $R^{+-}(\mathbf{r},\mathbf{r}';\omega)$ by projecting its imaginary part from left and right to a plane wave $e^{\mathrm{i}\mathbf{q}\cdot\mathbf{r}}$ giving $\mathrm{Im}\,R^{+-}(\mathbf{q},\omega)$ (Lowde et al. 1983). Sharp peaks in this function correspond to collective spin excitations, the spin waves, with wavevector $\mathbf{q}$ and frequency ω. Plotting the respective ω values against $\mathbf{q}$ yields the dispersion relation of the spin-wave mode. We note that another possibility is to perform a normal mode analysis of the imaginary part of R^{+-}, in matrix notation $\mathrm{Im}\,R^{+-} = (R^{+-} - R^{+-\dagger})/(2\mathrm{i})$.

4 Goldstone Condition

The Goldstone theorem states that the spontaneously broken spin-rotation symmetry in ferromagnetic materials leads to the appearance of a gapless magnon dispersion curve, i.e., the excitation energy vanishes in the limit $\mathbf{q} \to \mathbf{0}$. This has a very simple

physical explanation. The generating field is a magnetic field perpendicular to the ferromagnetic spin alignment, and it is commensurate with the unit cell in the limit $\mathbf{q} \to \mathbf{0}$. If the $\mathbf{B}$ field has a suitable shape in real space, it can act to rotate all electron spins collectively toward the field direction, i.e., the electron spins point in the same direction at all times. In the absence of spin-orbit coupling, this rigid rotation takes place without a cost of energy; hence $\omega = 0$. The pole at $\omega = 0$ corresponds to the long-wavelength limit of the acoustic magnon branch (Moriya 1985), identified as the *Goldstone mode*.

A rigid rotation of all spins does not change any relative spin alignment. The total energy calculated from the Heisenberg model is therefore invariant with respect to such a rotation, and the Goldstone condition is fulfilled identically. However, in the advanced methods based on TDDFT or MBPT, where the excitation energies define the pole structure of a two-particle propagator, the situation is much less transparent. We already know that the collective excitations arise from the nodes of the denominator of Eq. (44). (There is a very similar equation in TDDFT (Buczek et al. 2009; Lounis et al. 2010).) So, to be fulfilled, the Goldstone condition requires KW to have an eigenvector with eigenvalue 1 in the limits $\mathbf{q} \to \mathbf{0}$ and $\omega \to 0$. (We omit the indices in this section for simplicity.) Any numerical inaccuracy will lead to a slight deviation of the respective eigenvalue from 1 and, as a consequence, to a violation of the Goldstone condition. Often, this problem is circumvented by using the Goldstone criterion to fix a free parameter of the numerical scheme, thus, making a virtue of necessity. This free parameter has been chosen to be the effective interaction (Kotani and van Schilfgaarde 2008; Karlsson and Aryasetiawan 2000), the exchange-correlation kernel (Lounis et al. 2010, 2011), the bare susceptibility (Rousseau et al. 2012), or a scaling factor for the screened Coulomb interaction (Şaşıoğlu et al. 2010; Friedrich et al. 2014). Another possibility is an a posteriori correction of the resulting susceptibility (Buczek 2009; Buczek et al. 2009, 2011). However, in our case, such a pragmatic approach seems inappropriate. There is no mistaking that W is the RPA screened interaction Eqs. (13) and (14) and K is the two-particle propagator Eq. (25). So, strictly speaking, there is no room or justification for introducing a free parameter. Therefore, we analyzed the problem in more detail in Müller et al. (2016). We argued that there is an inconsistency between the free propagator G (and, hence, K) and the screened interaction W, and it is this inconsistency that is responsible for the Goldstone violation. In this chapter, we go a step further and present a mathematical proof that constructing the single-particle propagator from a self-consistent Coulomb-hole screened-exchange (COHSEX) self-energy (Hedin 1965, 1999) should revoke the inconsistency provided that a complete basis is used for the solution of the Bethe-Salpeter equation (Eq. (32)). However, the Wannier basis and, in particular, the on-site approximation do not fulfill the latter criterion so that a finite gap error must still be expected in our approach. Nevertheless, numerical results for the bulk $3d$ transition metals iron, cobalt, and nickel show that the Goldstone violation is substantially reduced if the propagator is self-consistently renormalized with the COHSEX self-energy. In practice, the application of the COHSEX self-energy is considerably more time-consuming than standard LSDA calculations. Therefore, we discuss a correction

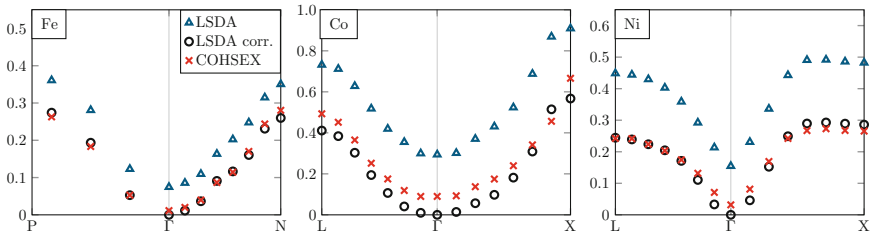

Fig. 3 Spin-wave spectra for Fe, Co, and Ni obtained with the LSDA (blue triangles), corrected LSDA (black circles), and COHSEX (red crosses) Green functions as starting point. (Müller et al. (2016) Copyright 2016 American Physical Society)

scheme for the LSDA Green function of ferromagnetic materials, ultimately introducing a free parameter as a pragmatic and efficient solution. We show that the corrected LSDA magnon spectra for the 3*d* transition metals iron, cobalt, and nickel are close to the results obtained from the much more expensive COHSEX approach.

In the following, we discuss the spin-wave spectra for the elementary bulk ferromagnets Fe, Co, and Ni with regard to the starting-point dependence of MBPT. We refer here to the Green function used in Eqs. (14) and (25). Since a set of single-particle states is already available from the ground-state calculation, a convenient choice is the LSDA Green function calculated from the corresponding Kohn-Sham wave functions and energies. We have used Wannier functions of *s*, *p*, and *d* character constructed from the 18 lowest Kohn-Sham bands. The resulting spin-wave dispersions for all three materials are shown as the blue symbols in Fig. 3, correctly showing a quadratic behavior around the Γ point. However, they also clearly exhibit a violation of the Goldstone theorem: the spin-wave excitation energy does not vanish in the center of the BZ as it should.

There are a number of approximations used in our numerical approach, which might be responsible for this violation, e.g., the on-site approximation, the incompleteness of the Wannier basis, convergence issues (**k**-point set, basis sets, empty-state summations), and so on. Apart from these, there is another more fundamental inconsistency in the chosen approach, which we will investigate in the following. This inconsistency concerns the choice of the starting point, i.e., the LSDA Green-function propagator. Equation (44) is derived under the assumption that the Green function be self-consistently renormalized with the GW self-energy. Only if this condition is fulfilled do we obtain the infinite series of ladder diagrams shown in Fig. 1. The two quantities, G and W, are thus related, and one must be chosen in accordance with the other.

Unfortunately, fully self-consistent GW calculations for transition-metal bulk systems are nowadays still a major challenge due to the dense **k**-point sets that are needed. On a second thought, however, we should also remember the static approximation that we have applied to W. For this reason, the proper self-energy to be used in the framework of our theoretical approach would have to be constructed

with the static screened interaction. An obvious choice would be the Coulomb-hole screened-exchange (COHSEX) self-energy (Hedin 1965, 1999), in which the dynamical W is replaced by the static $W(\mathbf{r}, \mathbf{r}') = W(\mathbf{r}, \mathbf{r}'; \omega = 0)$. It consists of two terms, the screened exchange (SEX) and the Coulomb-hole (COH) term. The former corresponds to Hartree-Fock theory with the bare Coulomb interaction replaced by $W(\mathbf{r}, \mathbf{r}')$

$$\Sigma^{\sigma}_{\mathrm{SEX}}(\mathbf{r}, \mathbf{r}') = -n^{\sigma}(\mathbf{r}, \mathbf{r}')W(\mathbf{r}, \mathbf{r}') \tag{49}$$

with the density matrix $n^{\sigma}(\mathbf{r}, \mathbf{r}') = \sum_{\mathbf{k}}^{\mathrm{BZ}} \sum_{n}^{\mathrm{occ}} \varphi^{\sigma}_{\mathbf{k}n}(\mathbf{r})\varphi^{\sigma *}_{\mathbf{k}n}(\mathbf{r}')$. The latter is given by

$$\Sigma_{\mathrm{COH}}(\mathbf{r}, \mathbf{r}') = \frac{1}{2}\delta(\mathbf{r} - \mathbf{r}')[W(\mathbf{r}, \mathbf{r}') - v(\mathbf{r}, \mathbf{r}')]\,, \tag{50}$$

which acts as a local and spin-independent potential. It accounts for the interaction energy of a quasiparticle with its induced (static) polarization cloud. Therefore, this term only couples charge degrees of freedom (if spin-orbit coupling is set aside) and does not affect the linear response of transversal spin fluctuations. Only Eq. (49), corresponding to Eq. (12) with $W(\mathbf{r}, \mathbf{r}'; \tau + \eta)$ replaced by $W(\mathbf{r}, \mathbf{r}')$, contributes to the right-hand side of Eq. (16) with $\delta\Sigma/\delta G = \mathrm{i}W(0)$. Obviously, this leads to the same form of the Bethe-Salpeter equation as before.

Up to now, our argumentation was based on "theoretical consistency." In the following, we analyze the Goldstone criterion in a mathematical way starting from Eq. (44) (or the more general Eq. (32)), in which all quantities are four-point functions, and $-2R^{(4)}$ and $-2K$ must be understood in the general sense that they give the response of the magnetic density matrix $m^{+}(\mathbf{r}, \mathbf{r}'; \omega)$ with respect to changes of a nonlocal magnetic field $B^{+}(\mathbf{r}, \mathbf{r}'; \omega)$ in the interacting and noninteracting system, respectively. Conversely, the expression $(-2R^{(4)})^{-1}\Delta m^{+}$ gives the perturbing field $\Delta B^{+}(\mathbf{r}, \mathbf{r}'; \omega)$ that would generate the change of the magnetization $\Delta m^{+}(\mathbf{r}, \mathbf{r}; \omega)$. For the Goldstone mode in the limit $\omega \to 0$, we know that a rigid rotation of the electron spins, i.e., $\Delta m^{+} \propto m$, can take place even without a perturbing field. So, we have $(-2R^{(4)})^{-1}m = 0$, and with Eq. (44) we can write $KWm = m$. The eigenfunction of KW with eigenvalue 1 is, thus, revealed to be the magnetization density (matrix). We claim that this condition is fulfilled if COHSEX is taken for the starting point. When separating off the spin-independent part of Eq. (49), the remaining spin-dependent part can formally be interpreted as a nonlocal magnetic field

$$B(\mathbf{r}, \mathbf{r}') = -\frac{1}{2}W(\mathbf{r}, \mathbf{r}')[n^{\uparrow}(\mathbf{r}, \mathbf{r}') - n^{\downarrow}(\mathbf{r}, \mathbf{r}')] = -\frac{1}{2}W(\mathbf{r}, \mathbf{r}')m(\mathbf{r}, \mathbf{r}')\,. \tag{51}$$

Now we use the simple fact that rigidly rotating the **B** field that creates the magnetization in a noninteracting system will rotate the magnetization in the same way, which can be expressed as

$$m(\mathbf{r},\mathbf{r}') = -2\iint K(\mathbf{r},\mathbf{r}';\mathbf{r}'',\mathbf{r}''')B(\mathbf{r}'',\mathbf{r}''')d\mathbf{r}''d\mathbf{r}''' \,. \tag{52}$$

(For the rotation to be rigid, $\Delta B^+ \propto B$, and the corotation of B field and magnetization requires $\Delta B^+/B = \Delta m^+/m$.) The assertion then follows from inserting Eq. (51) into Eq. (52).

The proof is already complete, but it is helpful to show $KWm = m$ more explicitly. In the limit $\omega \to 0$, the imaginary part of the two-particle propagator Eq. (34) is zero, and we can write

$$K(\mathbf{r},\mathbf{r}';\mathbf{r}'',\mathbf{r}''') = \frac{1}{N^2}\sum_{\mathbf{k},\mathbf{k}'}\sum_{m,m'}(f^{\downarrow}_{\mathbf{k}m} - f^{\uparrow}_{\mathbf{k}'m'})\frac{\varphi^{\downarrow}_{\mathbf{k}m}(\mathbf{r})\varphi^{\downarrow *}_{\mathbf{k}m}(\mathbf{r}'')\varphi^{\uparrow *}_{\mathbf{k}'m'}(\mathbf{r}')\varphi^{\uparrow}_{\mathbf{k}'m'}(\mathbf{r}''')}{\varepsilon^{\uparrow}_{\mathbf{k}'m'} - \varepsilon^{\downarrow}_{\mathbf{k}m}} \tag{53}$$

with the occupation numbers $f^{\sigma}_{\mathbf{k}m}$. [We have used $\sum_m^{\text{occ}}\sum_{m'}^{\text{unocc}}\ldots = \sum_{m,m'} f^{\sigma}_{\mathbf{k}m}(1-f^{\sigma}_{\mathbf{k}m'})\ldots = \sum_{m,m'} f^{\sigma}_{\mathbf{k}m}\ldots$.] Because of Eq. (51) the COHSEX single-particle Hamiltonian fulfills $H^{\downarrow} - H^{\uparrow} = Wm$, which gives

$$\begin{aligned}\iint KWm &= \frac{1}{N^2}\sum_{\mathbf{k},\mathbf{k}'}\sum_{m,m'}(f^{\downarrow}_{\mathbf{k}m} - f^{\uparrow}_{\mathbf{k}'m'})\frac{\varphi^{\downarrow}_{\mathbf{k}m}(\mathbf{r})\langle\varphi^{\downarrow}_{\mathbf{k}m}|H^{\downarrow} - H^{\uparrow}|\varphi^{\uparrow}_{\mathbf{k}'m'}\rangle\varphi^{\uparrow *}_{\mathbf{k}'m'}(\mathbf{r}')}{\varepsilon^{\uparrow}_{\mathbf{k}'m'} - \varepsilon^{\downarrow}_{\mathbf{k}m}} \\ &= \frac{1}{N}\sum_{\mathbf{k}}\sum_{m,m'}(f^{\uparrow}_{\mathbf{k}m'} - f^{\downarrow}_{\mathbf{k}m})\varphi^{\downarrow}_{\mathbf{k}m}(\mathbf{r})\langle\varphi^{\downarrow}_{\mathbf{k}m}|\varphi^{\uparrow}_{\mathbf{k}m'}\rangle\varphi^{\uparrow *}_{\mathbf{k}m'}(\mathbf{r}') = m(\mathbf{r},\mathbf{r}').\end{aligned} \tag{54}$$

That the last expression is really the spin density matrix is seen by expanding $\varphi^{\uparrow}_{\mathbf{k}m'}(\mathbf{r})$ and $\varphi^{\downarrow *}_{\mathbf{k}m}(\mathbf{r})$ in terms of the functions of the other spin channel

$$\begin{aligned}m(\mathbf{r},\mathbf{r}') &= \frac{1}{N}\sum_{\mathbf{k}}\sum_{m'} f^{\uparrow}_{\mathbf{k}m'}\varphi^{\uparrow}_{\mathbf{k}m'}(\mathbf{r})\varphi^{\uparrow *}_{\mathbf{k}m'}(\mathbf{r}') - \frac{1}{N}\sum_{\mathbf{k}}\sum_{m} f^{\downarrow}_{\mathbf{k}m}\varphi^{\downarrow}_{\mathbf{k}m}(\mathbf{r})\varphi^{\downarrow *}_{\mathbf{k}m}(\mathbf{r}') \\ &= \frac{1}{N}\sum_{\mathbf{k}}\sum_{m,m'}(f^{\uparrow}_{\mathbf{k}m'} - f^{\downarrow}_{\mathbf{k}m})\varphi^{\downarrow}_{\mathbf{k}m}(\mathbf{r})\varphi^{\uparrow *}_{\mathbf{k}m'}(\mathbf{r}')\langle\varphi^{\downarrow}_{\mathbf{k}m}|\varphi^{\uparrow}_{\mathbf{k}m'}\rangle \,.\end{aligned} \tag{55}$$

In Müller et al. (2016), we reported on spin-wave calculations based on the COHSEX Green function. Technically, we start from the mean-field LSDA solution and construct the LSDA Green function, the corresponding polarization function Eq. (14), and the static screened interaction Eq. (13), from which the COHSEX self-energy Eqs. (49) and (50) is evaluated. The latter is a Hermitian operator defining a new mean-field system. This allows the respective single-particle equations of motion to be solved in a similar way as the Kohn-Sham equations of DFT. To be more precise, the single-particle equations are iteratively solved until the density is converged. This process updates the density and, consequently, the Hartree potential in each iteration, while the COHSEX self-energy matrix remains fixed. This

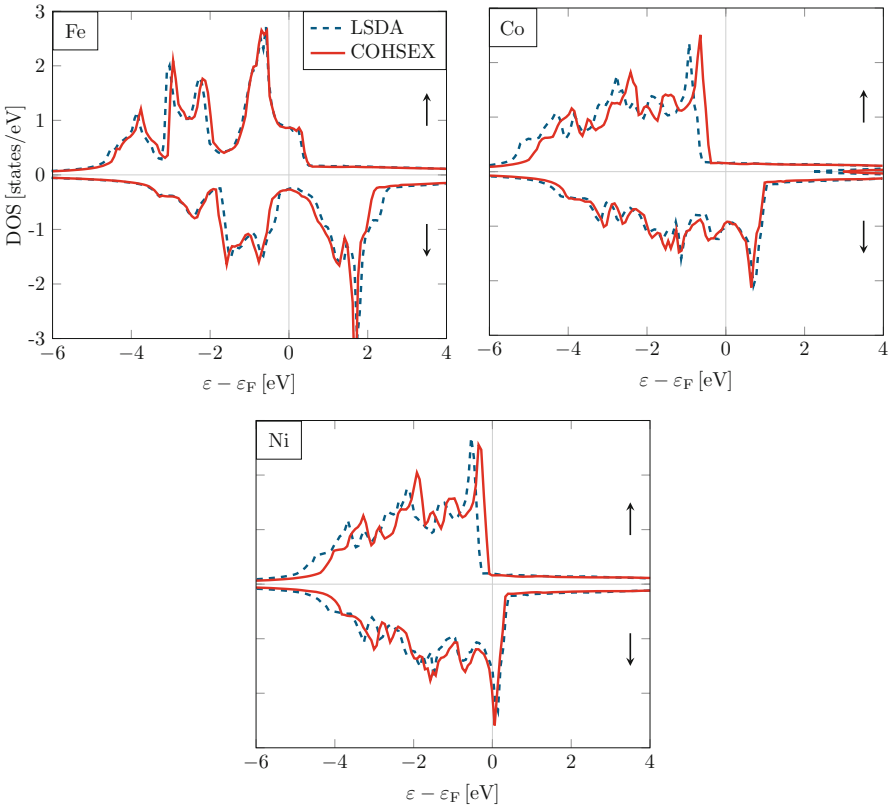

Fig. 4 DOS spectra for bulk Fe, Co, and Ni. The Fermi level is set to zero. (Müller et al. (2016) Copyright 2016 American Physical Society)

produces a new set of wave functions and energies that are then used to construct a new Green function and, ultimately, a new COHSEX self-energy matrix. The whole procedure is repeated until self-consistency is achieved. We have employed a $14 \times 14 \times 14$ **k**-point set for these calculations.

The mean-field solution of the 3*d* ferromagnets bcc iron, fcc cobalt, and fcc nickel based on the COHSEX self-energy is interesting in its own right. Figure 4 shows their densities of states (DOS) for both LSDA and COHSEX. At a first glance, the two DOS spectra look very similar for all materials. The COHSEX self-energy yields thus qualitatively the same correct result as LSDA: all three materials are ferromagnetic metals. There are however small quantitative differences. The occupied bandwidth shrinks, in particular for Co and Ni, and the spin-up and spin-down states show a relative energetic shift toward each other. This observation is confirmed by the exchange splittings of selected single-particle states listed in Table 1. The COHSEX values are systematically smaller than the LSDA ones, to the effect that the slight overestimation of the magnetic moment found in LSDA is

Table 1 Spin magnetic moments (obtained from a projection onto Wannier orbitals) and exchange splittings for selected states of Fe, Co, and Ni from LSDA, corrected LSDA, COHSEX, and experiment. (Müller et al. (2016) Copyright 2016 American Physical Society)

			LSDA	LSDA corr.	COHSEX	Experiment
m (μ_B)	Fe		2.20	2.16	2.11	2.08 (Stearns 1986; Bonnenberg et al. 1986)
	Co		1.62	1.49	1.46	1.52 (Stearns 1986; Bonnenberg et al. 1986)
	Ni		0.59	0.51	0.46	0.52 (Stearns 1986; Bonnenberg et al. 1986)
E_{ex} (eV)	Fe	Γ'_{25}	1.8	1.7	1.5	2.1 (Turner et al. 1984; Kisker et al. 1985; Sakisaka et al. 1985; Santoni and Himpsel 1991)
		H_{25}	2.1	2.0	1.7	1.8 (Santoni and Himpsel 1991)
		P_4	1.4	1.3	1.1	1.5 (Eastman et al. 1980)
	Co	Γ'_{12}	1.7	1.3	1.1	1.1 (Himpsel and Eastman 1980)
		Γ'_{25}	1.4	1.0	1.2	1.1 (Himpsel and Eastman 1980)
	Ni	L_3	0.5	0.3	0.4	0.3 (Eastman et al. 1980)
		X_2	0.6	0.4	0.3	0.2 (Raue et al. 1984)

corrected to smaller values in COHSEX, albeit somewhat too strongly in the case of Co and Ni. With the exception of iron, the exchange splittings are improved by the self-consistent COHSEX calculation, most notably for Ni, whose exchange splitting is known to be overestimated in LSDA.

Figure 3 shows the spin-wave dispersion calculated from the COHSEX Green function as red symbols. Employing the self-consistent COHSEX mean-field solution as starting point, in fact, decreases the gap error systematically compared to the corresponding LSDA values. In case of bcc iron, fcc cobalt, and fcc nickel, the error is reduced by 85%, 69%, and 79%, respectively.

The ansatz presented so far is computationally very demanding. It requires the self-consistent calculation of the COHSEX self-energy on a fine $\mathbf{k}$-point set. On the other hand, aside from the gap error, the magnon dispersions obtained from LSDA are very similar to the corresponding COHSEX results. This raises the question if it is possible to correct the LSDA Green function in a simple way that respects the Goldstone condition. In fact, this is possible.

Our approach is motivated by studying spin-wave solutions (Moriya 1985) of the one-band Hubbard model. When solved in the Hartree-Fock approximation, we obtain the magnetic susceptibility as a simple algebraic expression in the same form as Eq. (44) with the W matrix replaced by the Hubbard interaction parameter U. In the Goldstone limit, the two-particle propagator simplifies to $K = m/E_{ex}$ with the site magnetization m and the exchange splitting E_{ex}, and the Goldstone

condition can be phrased in the form of the simple relation $Um/E_{\mathrm{ex}} = 1$. To remain consistent, we have to evaluate K in the Hartree-Fock mean-field system, in which case $E_{\mathrm{ex}} = Um$, and the Goldstone condition is identically fulfilled. The simple form of the relation invites one to use one of the constituent quantities as an adjustable parameter. The U parameter plays the role of the screened interaction W, which is a matrix and thus cannot be corrected easily by a single parameter. Besides, we obtain W from a many-body treatment of screening, and it does not seem appropriate to correct it in such an ad hoc way. Second, the magnetization m results from the self-consistent LSDA calculation and cannot be varied straightforwardly. At last, E_{ex} can be regarded as the energy difference between the spin-up and spin-down electron bands, which can easily be varied once a self-consistent LSDA solution has been found. Moreover, this correction will specifically modify the LSDA Green function, which was our intention, while leaving the screened interaction unchanged. The correction can be hoped to mimic to some extent the missing renormalization in the Green function. Therefore, we choose E_{ex} as an adjustable parameter. To be more precise, we rigidly shift the spin-up and spin-down states relative to each other $\varepsilon_{\mathbf{k}m}^{\uparrow/\downarrow} \to \varepsilon_{\mathbf{k}m}^{\uparrow/\downarrow} \pm \Delta E_{\mathrm{ex}}/2$ until the Goldstone condition is fulfilled. The LSDA Green function corrected in this way is then used to construct the two-particle propagator K. This procedure yields magnon dispersions, which respect the Goldstone condition and are close to the COHSEX results for the three materials as shown in Fig. 3. The relative shift in the band energies is such that the exchange splittings decrease. For Fe, Co, and Ni, we find $\Delta E_{\mathrm{ex}} = 0.10\,\mathrm{eV}$, $\Delta E_{\mathrm{ex}} = 0.39\,\mathrm{eV}$, and $\Delta E_{\mathrm{ex}} = 0.21\,\mathrm{eV}$. The Fermi energy is adjusted accordingly so that the correction affects the ground-state magnetic properties as well. Interestingly, the resulting magnetic moments and exchange splittings turn out to be close to the corresponding COHSEX values listed in Table 1. They also compare well with experiment. The proximity of COHSEX and corrected LSDA values can be regarded as an a posteriori justification of the correction. Among the three materials, fcc cobalt appears as a problematic case. The gap error is largest and the COHSEX spin-wave dispersion shows an unusually flat behavior at the Γ point. In fact, the curvature there is very small, being between results from LSDA (small positive curvature) and PBE (small negative curvature, not shown), indicative of a magnetic instability. This is in accordance with previous DFT results. Janak (1978) found that there are two competing magnetic ground states with low and high magnetic moment, and Moruzzi et al. (1986) report an unusually strong dependence of the magnetic properties on the lattice constant.

The findings can be interpreted in a more fundamental way. Formally, the Hamiltonian which describes the magnetic system is invariant with respect to spin rotations, while the ferromagnetic ground state is not. This implies the existence of a gapless excitation due to a homogeneous magnetic perturbation perpendicular to the magnetization axis. Baym and Kadanoff (1961) and Baym (1962) formulated a conserving and self-consistent scheme for correlation functions. The scheme was extended by Brandt et al. (Brandt et al. 1970, 1971; Brandt 1971) to the magnetic case. They showed that for a spin-conserving formulation of the magnetic susceptibility, which fulfills the Goldstone theorem automatically, several conditions

have to be fulfilled. The chosen self-energy approximation is to be calculated self-consistently with the Green function. This ensures that the single-particle states which form the basis for the electron-hole propagator are consistent with the applied self-energy approximation. In addition, the spin-independent interaction that is responsible for the correlation among the electron-hole pairs with opposite spins is required to be consistent with the self-energy as these properties are connected via $\delta\Sigma/\delta G = \mathrm{i}W$. If both conditions are fulfilled, the magnetic response function will fulfill the Goldstone theorem. Then, the electron-hole pair propagator and the screened interaction are compatible with the Ward identity ensuring spin conservation. In particular, the correct limit $\mathbf{q} \to \mathbf{0}$ is attained.

5 Spin Excitation Spectra

In this section, we present detailed results of first-principles calculations for the three bulk transition metals Fe, Co, and Ni. The properties of these materials are strongly governed by the presence of the localized $3d$ states. It is the exchange interaction among the $3d$ electrons that drives the systems into the ferromagnetic ground state. On the other hand, the materials are metallic. The $3d$ states of neighboring atoms overlap, and there is a partly filled itinerant $4s$ band which spans the entire valence region and mixes with the d bands. As a consequence, Fe, Co, and Ni show signatures of itinerant magnetism. For example, they fulfill the Stoner criterion of ferromagnetism, and there is no order-disorder phase transition at the Curie temperature as would be described by the Heisenberg model.

So, one would expect these bulk transition metals to show both localized and itinerant magnetic behavior. The present formalism using MBPT is capable of describing both types of magnetism on the same footing. The spectrum of spin excitations in this theory is given by the imaginary part of the magnetic response function as calculated from Eqs. (28) and (44). The poles of this function lie infinitesimally below (above) the positive (negative) real-frequency axis, and they come from both the two-particle propagator (bare susceptibility) in the numerator and the roots of the denominator. In the former case, the spin excitations have a single-particle character. These Stoner excitations can be described as excitations of single electrons across the Fermi surface with an accompanying spin flip of the electrons. In the latter case, the excitations are collective in nature, again with a total spin flip of 1, and arise from superpositions of infinitely many electron-hole pairs (single-particle excitations) coupled to each other by the exchange interaction. These electron-hole pairs describe changes in the spin density, in which all electrons take part collectively and which can, for example, have the form of spin waves. The two types of excitations are just limiting cases. In general, the spin excitations have a mixed character of single-particle and collective excitations: spin waves acquire a finite lifetime through a coupling to Stoner excitations, and Stoner excitations lose or gain spectral weight by a coupling to spin waves.

It is instructive to consider the model of a homogeneous electron gas with spin polarization. The spin-up and spin-down bands have the form of free-electron bands,

but they are shifted with respect to each other by the exchange splitting E_{ex}, i.e., $\varepsilon_{\mathbf{k}}^{\sigma} = k^2 - \sigma E_{\mathrm{ex}}/2$. Energies and momenta are in units of the Fermi wavevector k_0 and Fermi energy $\varepsilon_0 = k_0^2/2$ of the paramagnetic system, respectively. The bare susceptibility of this system can be calculated from Eqs. (34) and (47) in a pure plane-wave representation. To simplify the evaluation of $K^{\downarrow\uparrow}$, we replace $-\mathrm{i}\eta$ in the first term by $+\mathrm{i}\eta$, which amounts to using the corresponding retarded quantity. This enables a straightforward integration over the occupied spin-up and spin-down band (Moriya 1985) yielding

$$K^{+-}(q,\omega) = \frac{-1}{4\pi^2 q} \sum_{\sigma=-1}^{1} \sigma \left[\frac{1}{2}(p_\sigma^2 - k_\sigma^2) \left(\ln \left| \frac{p_\sigma + k_\sigma}{p_\sigma - k_\sigma} \right| + \mathrm{i}\pi \,\mathrm{sgn}(\omega)\theta(k_\sigma - |p_\sigma|) \right) - p_\sigma k_\sigma \right] \tag{56}$$

with $p_\sigma = (\omega - \sigma q^2 - E_{\mathrm{ex}})/(2q)$, the spin-dependent Fermi wavevector $k_\sigma = (1+\sigma\zeta)^{1/3}$, the exchange splitting $E_{\mathrm{ex}} = (1+\zeta)^{2/3} - (1-\zeta)^{2/3}$, the spin polarization $\zeta = M/N = (k_\uparrow^3 - k_\downarrow^3)/(k_\uparrow^3 + k_\downarrow^3)$, and the Heaviside function $\theta(x) = 1$ for $x > 0$ and 0 for $x < 0$. The factor $\mathrm{sgn}(\omega)$ has been introduced to undo the sign change $-\mathrm{i}\eta \to +\mathrm{i}\eta$, which recovers the time-ordered two-particle propagator. All quantities can be written in terms of a single parameter, the spin polarization $\zeta \in [0, 1]$.

The area where the imaginary part of $K^{+-}(q,\omega)$ is nonzero defines the Stoner continuum, which, by using the definition of θ, can be shown to be bounded by the functions $2qk_\sigma + \sigma q^2 + E_{\mathrm{ex}}$ from above and $-2qk_\sigma + \sigma q^2 + E_{\mathrm{ex}}$ from below. Figure 5 presents a plot of $-\operatorname{Im} K^{+-}(\mathbf{q},\omega)$ together with the boundary lines for a spin-polarized electron gas with $\zeta = 0.9$. The imaginary part diverges for $\omega = E_{\mathrm{ex}} = 1.32$ and $q \to 0$, because the real part of the denominator of Eq. (34) vanishes in this limit. We also see that the Stoner continuum extends toward negative energies. This is because, as long as $\zeta < 1$, there can be transitions from occupied minority to unoccupied majority bands. At $\omega = 0$, the imaginary part of K^{+-} is zero for all momenta because the phase space of single-particle excitations vanishes in this limit.

Of course, the homogeneous electron gas is a relatively crude model. The absence of the crystal field and of atomic wave functions makes one wonder whether this model could be just too simple. Therefore, it is interesting to compare Fig. 5a to corresponding plots calculated with realistic wave functions and energies from a self-consistent Kohn-Sham solution. In particular, we have calculated the bare susceptibility from Eq. (48) and projected it onto the plane wave $e^{\mathrm{i}\mathbf{q}\cdot\mathbf{r}}$ from both sides giving $K^{+-}(\mathbf{q},\omega)$. A fine $20 \times 20 \times 20$ $\mathbf{k}$-point grid was employed, and the Wannier basis was the same as in Sect. 4. We have also applied the E_{ex} correction. The plots for bcc Fe, fcc Co, and fcc Ni are presented in Fig. 6a–c. It is surprising that they share a number of similarities with the plot for the homogeneous electron gas. First, the maximum of $-\operatorname{Im} K^{+-}(\mathbf{q},\omega)$ is seen for $\omega \approx E_{\mathrm{ex}}$ and $\mathbf{q} = \mathbf{0}$. In

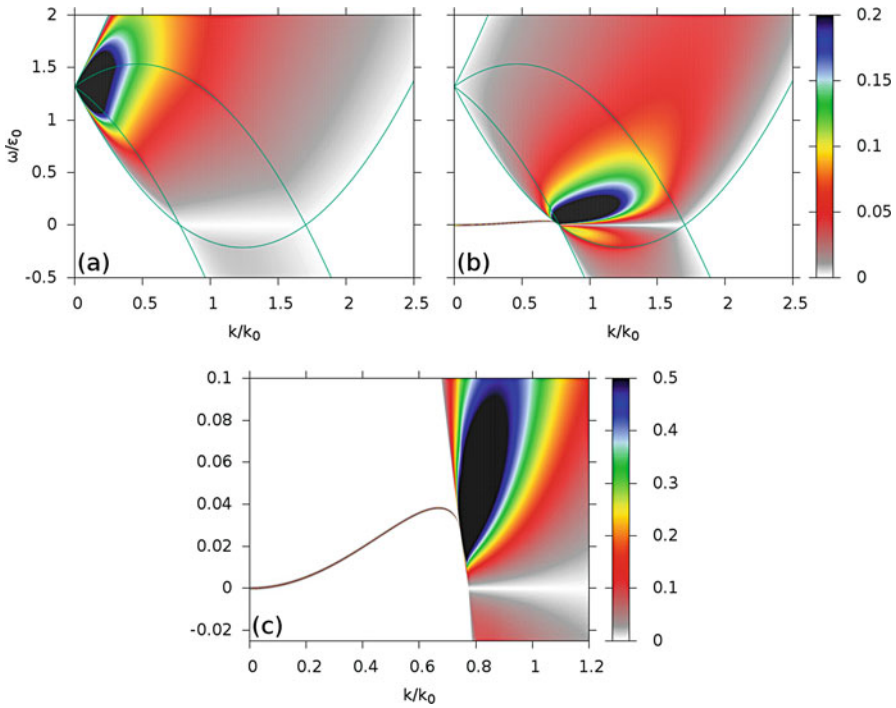

Fig. 5 Imaginary part of (**a**) the bare $[-\operatorname{Im} K^{+-}(\mathbf{q},\omega)]$ and (**b**) the renormalized susceptibility $[-\operatorname{Im} R^{+-}(\mathbf{q},\omega)]$ for the homogeneous electron gas with spin polarization $\zeta = 0.9$; (**c**) is a magnification of (**b**). The green solid lines show the boundaries of the Stoner continuum. In (**b**) and (**c**), a finite imaginary frequency of, respectively, $\mathrm{i}\eta = \mathrm{i}10^{-5}$ and $\mathrm{i}\eta = \mathrm{i}10^{-7}$ has been employed in order to make the magnon branch visible, which would have a vanishing (delta-like) width in this system otherwise

contrast to before, there is no divergence because spin-up and spin-down bands have different dispersions in a real material, and the majority bands shifted up by E_{ex} thus cannot coincide exactly with the minority bands, in particular, since E_{ex} is not a unique quantity but $\mathbf{k}$ dependent. Consequently, the maximum at $\mathbf{q} = \mathbf{0}$ has a certain width in energy. Furthermore, as before, we observe a weak intensity of Stoner excitations for negative ω. As a qualitative difference to Fig. 5, the spectra of Co and Ni exhibit a horizontal, nearly dispersion-less band of high intensity that emanates from the maximum at Γ and stretches toward the X point. This feature can be directly related to the localized nature of the single-particle states. The densities of d states of Co and Ni show particularly sharp peaks in the majority valence and minority conduction regions separated by 1.3 and 0.5 eV, respectively, revealing the feature to originate from single-particle $d \to d$ transitions.

There are no clear boundary lines as for the homogeneous electron gas beyond which the imaginary part of K^{+-} would vanish. In fact, there can be Stoner excitations for all $\mathbf{q}$ and ω (except for $\omega = 0$). However, the form of $-\operatorname{Im} K^{+-}(\mathbf{q},\omega)$ is

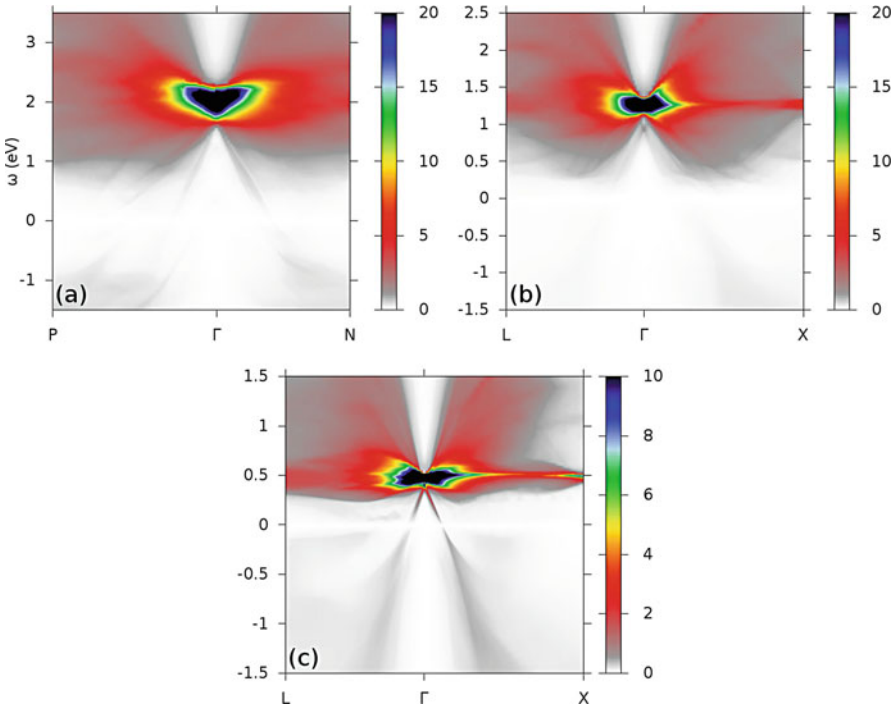

Fig. 6 Imaginary part of the bare susceptibility $[-\operatorname{Im} K^{+-}(\mathbf{q}, \omega)$ in units of $(\Omega \mathrm{eV})^{-1}$; Ω = unit-cell volume] for (**a**) bcc Fe, (**b**) fcc Co, and (**c**) fcc Ni as a function of $\mathbf{q}$ and ω

definitely similar. In particular, the characteristic V-shaped regions with (nearly) no excitations above and below the maximum are present, and, instead of the boundaries, one observes *stripes* of increased intensity seemingly extending from the maximum. A pronounced one is seen in the spectrum of Ni. These stripes will play an important role in the renormalized spectra later on. They can be understood by realizing that the function $-\operatorname{Im} K^{+-}(q, \omega)$ can roughly be thought of as giving the intersection of the valence majority states shifted upward by ω and sideways by $-\mathbf{q}$ with the conduction minority states. This is illustrated in Fig. 7 where the electronic bands are assumed to show a linear dispersion at finite q. Starting from the (near) coincidence of the bands at $q = 0$ and $\omega = E_{\mathrm{ex}}$, relatively large intensities are still expected when the majority band is shifted from there in such a way that the regions of linear dispersion remain overlapping, giving rise to the condition of proportionality $\omega \propto q$ and, hence, to the stripes. Here, we have assumed that the spin-up band is filled, while the spin-down band is empty and that they exhibit similar dispersions as is often the case in ferromagnets. Even in the case of the highly symmetric homogeneous electron gas, whose bands exhibit a constant curvature and no linear dispersions as in Fig. 7, the onset of the Stoner continuum at the boundaries is quite abrupt. So, it is not surprising that real materials show more structure there.

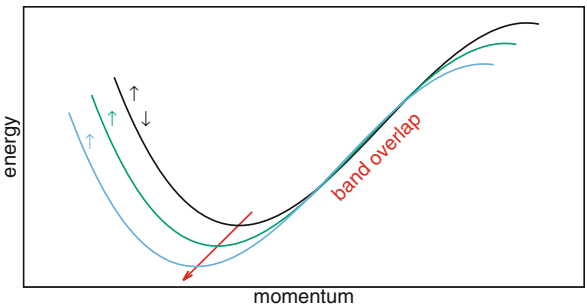

Fig. 7 Illustration of the "band overlap" leading to the striped Stoner continuum of Fig. 6. The red arrow denotes the proportionality $\omega \propto q$

Up to now, we have discussed the spin excitation spectrum of the fictitious noninteracting reference system. The spectrum changes profoundly when one introduces a finite interaction among the electrons. In the case of the homogeneous electron gas, one would have to solve the Bethe-Salpeter equation $R^{+-}(q,\omega) = K^{+-}(q,\omega)/[1 - WK^{\downarrow\uparrow}(q,\omega)]$ with $K^{\downarrow\uparrow}(q,\omega) = -K^{+-}(q,\omega)/2$ (cmp. Eq. (47)) and a so-far unknown effective interaction W. The latter is a single parameter in this case and can be obtained conveniently from the Goldstone condition, giving $W = 1/K^{\downarrow\uparrow}(0,0) = -2/K^{+-}(0,0) = 3\pi^2 E_{\mathrm{ex}}/\zeta$. The spin excitation spectrum is then given by $-\operatorname{Im} R^{+-}(\mathbf{q},\omega)$ shown in Fig. 5b for the homogeneous electron gas. Together with the spectrum, we have plotted the boundary lines of the Stoner continuum as solid green lines. Still, these lines separate the regions of finite intensity from the regions of no intensity, except for the spin-wave branch, which starts at the origin $q = \omega = 0$ and disperses quadratically for small q according to $\omega \propto Dq^2$ with $D = [1 - 0.4(k_\uparrow^5 - k_\downarrow^5)/(k_\uparrow^2 - k_\downarrow^2)]/\zeta$ (Moriya 1985). For larger q, the magnon branch deviates from the parabolic dispersion and finally enters the Stoner continuum, where it couples to the Stoner excitations forming a broad maximum. The magnon energies are much smaller than E_{ex}, even for small E_{ex} because $D \sim E_{\mathrm{ex}}/12$ in this limit. Therefore, we show an enlarged picture of the magnon branch in Fig. 5c. We note that a finite (instead of infinitesimal) parameter $\eta = 10^{-5}$ and $\eta = 10^{-7}$ has been employed in (b) and (c), respectively, which leads to a corresponding finite linewidth of the magnon branch outside the Stoner continuum.

When comparing with Fig. 5a, we observe a strong redistribution of quasiparticle weight after solving the Bethe-Salpeter equation. In particular, the region of maximal intensity around $q = 0$ now appears very shallow, and a new maximum is found where the spin-wave branch enters the Stoner continuum. The former is a feedback effect: the transfer of spin-up electrons into the spin-down channel leads to a strong change in the exchange field of the interacting system, which acts against the transfer of electrons, an effect similar to the electronic screening effect. The new maximum comes from a resonance effect between the collective magnon and the Stoner excitations. The amplifying effect of the resonance extends into the Stoner excitations of negative energy ($\omega < 0$), which now appear more intense than in Fig. 5a. It is interesting to note that the maximum in Fig. 5a transforms continuously into the one of (b) if one smoothly varies the parameter W from 0 to $3\pi^2 E_{\mathrm{ex}}/\zeta$.

The spin-wave branch starts to appear for $W \gtrsim 0$ slightly below the maximum at $\omega = E_{\mathrm{ex}}$, and as W increases, it shifts down, first with a maximum at $q = 0$, then developing a minimum, until, for $W = 3\pi^2 E_{\mathrm{ex}}/\zeta$, it finally has the form of Fig. 5c. Further increasing W would shift the minimum of the magnon branch to negative energies. This again demonstrates how sensitive the Goldstone condition is and explains the difficulty of its fulfillment in first-principles calculations.

In Fig. 8a–c, we show the renormalized susceptibility for Fe, Co, and Ni, again projected onto $e^{\mathrm{i}\mathbf{q}\cdot\mathbf{r}}$. We have used the same scales as before to make a direct comparison possible. Obviously, the regions around the spin-wave branch have values exceeding the maximum of the color scale (black area). Therefore, Fig. 8d–f presents a magnified picture with a different color scale. As with the bare susceptibility, there are a number of similarities to Fig. 5b: a spin-wave branch is formed by the renormalization; this branch acquires a finite lifetime broadening by a coupling to Stoner excitations; the former intensity maximum around $\omega = E_{\mathrm{ex}}$ and $\mathbf{q} = \mathbf{0}$ has lost much of its intensity; there is a resonant enhancement of the Stoner intensity for $\omega < 0$. However, there are also some important differences to the case of the homogeneous electron gas. First, the coupling to Stoner excitations sets in much earlier, because the Stoner excitations are present at all energies. Nevertheless, the spin-wave dispersion remains discernible to quite large momenta and energies compared to the case of the homogeneous electron gas, indicating a localized nature of magnetism in these materials. Especially in Ni, the magnon branch seems to couple resonantly with the horizontal Stoner band toward the X point. While the spin-wave branches still have an overall parabolic shape, they show a rather irregular behavior, which can be attributed to the coupling to the Stoner continuum. In particular, in all cases the magnon branch is affected, sometimes interrupted, by the interaction with the *striped* Stoner spectrum we have discussed before. In fact, if we magnify the corresponding region of the spectrum for Ni (see inset in Fig. 8f), we can observe that the coupling between the magnon branch and a line of strong Stoner intensity – we could call it a *Stoner band* – leads to a feature that looks like an "avoided crossing." In fact, this feature has a similar origin as an avoided crossing of single-particle bands, with the difference that the two states that interact here are not single-particle but many-body states, the collective spin-wave excited state and a superposition of Stoner excitations, which mix and exchange character.

Despite the multiple interactions with the Stoner background, we find that the dispersion of the spin-wave branches is mostly isotropic in $\mathbf{q}$ space. The numerical data for iron are in qualitative and also quantitative agreement with the neutron scattering experiments of Collins et al. (1969), Mook and Nicklow (1973), and Lynn (1975), where spin-wave energies up to 70, 118, and 110 meV were reported, respectively; see Friedrich et al. (2014) for a comparison. In Loong et al. (1984), spin-wave resonances up to an energy of 160 meV could be measured. However, the latter experimental results partly disagree with the values of Mook and Nicklow (1973), especially at the high end of the spectrum. We also find good agreement in the case of nickel (Minkiewicz et al. 1969; Mook and Tocchetti 1979; Mook and Paul 1985), while neutron scattering data for cobalt is scarce and limited to small momentum transfers (Frikkee 1966; Glinka et al. 1977).

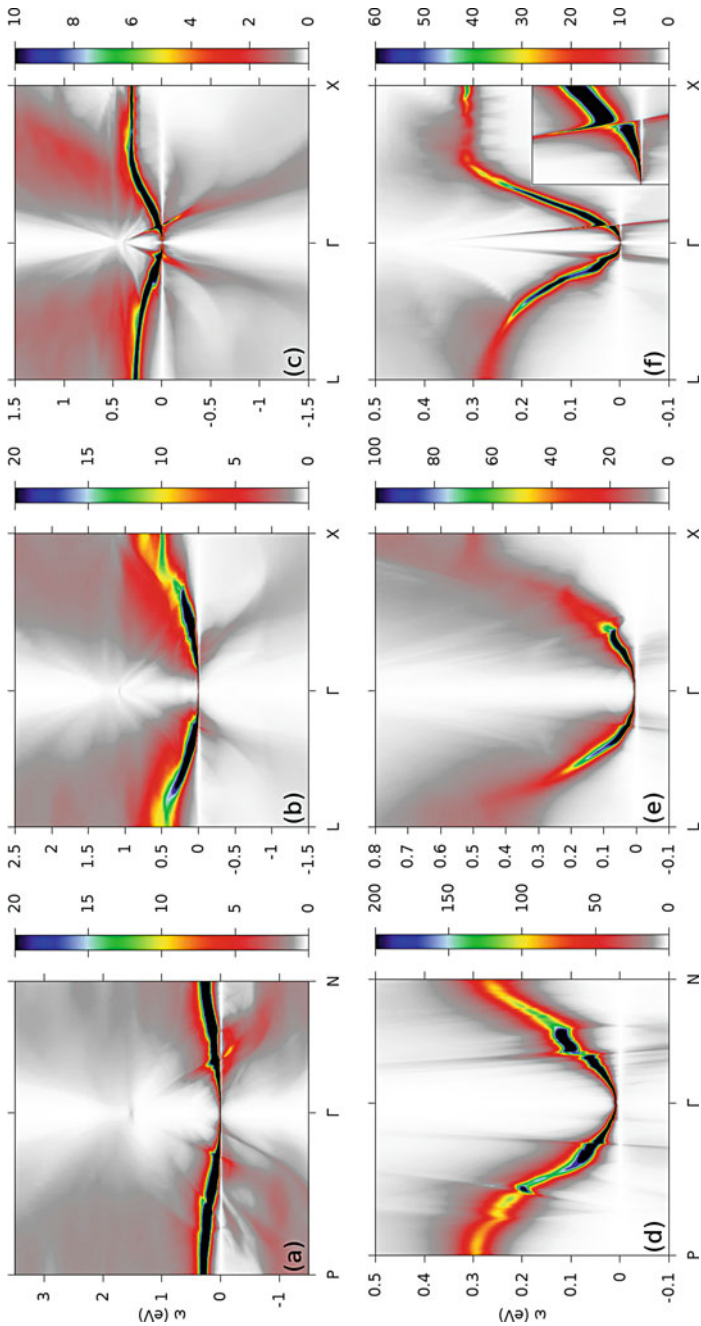

Fig. 8 Same as Fig. 6 for the renormalized susceptibility $[-\operatorname{Im} R^{+-}(\mathbf{q}, \omega)$ in units of $(\Omega \mathrm{eV})^{-1}]$; (**d**)–(**f**) are magnifications of (**a**)–(**c**) with different scales. The inset of (**f**) shows a magnified view of the region where the magnon branch couples to the increased Stoner intensity

A feature that has been discussed extensively in the literature (Cooke 1976; Mook and Tocchetti 1979; Cooke et al. 1980, 1985; Callaway et al. 1983; Mook and Paul 1985; Savrasov 1998; Karlsson and Aryasetiawan 2000; Şaşıoğlu et al. 2010; Friedrich et al. 2010) is the appearance of an "optical" spin-wave branch, in addition to the acoustic one, for example, in fcc Ni along $\Gamma-\mathrm{X}$. The terminology is, however, a little bit misleading, as the acoustic branch just seems to exhibit a gap at around 130 meV. The lower-energy end flattens and eventually disappears toward larger momenta (or persists out to the zone boundary (Cooke et al. 1985; Blackman et al. 1985)), and the higher-energy end then continues to form the acoustic magnon branch. The two ends coexist in a certain region of the reciprocal space giving a double-peak structure in the spectra there. This indicates the existence of an optical branch that crosses the acoustic branch and splits it into two pieces. The optical branch has yet to be observed directly, however. (In some publications, the higher-energy branch is denoted as the optical branch, although it does not extend to zero momentum and finite energy as in the case of optical phonon branches.) After its theoretical prediction (Cooke 1976), the optical branch was detected in the form of a double peak in constant $\mathbf{q}$ scans in neutron scattering experiments (Mook and Tocchetti 1979; Mook and Paul 1985). However, this feature seems to be an elusive phenomenon, which is observed in some studies (Cooke et al. 1985; Blackman et al. 1985) but not in others (Callaway et al. 1983).

In Fig. 8f, we clearly see a gap in the acoustic branch at around 30 meV, which arises from the coupling to Stoner excitations as we have seen before. But this gap is located at a too low energy and too close to the Γ point to be identified as the optical branch discussed in the literature. On the other hand, there is no gap to be seen in Fig. 8f at around 130 meV. However, if we analyze this part of the excitation spectrum more closely, we are able to identify two peaks, but these peaks do not appear as separate peaks in our calculation. They form a broad peak, and only a peak fit with Lorentzian functions reveals the existence of a lower-energy and a high-energy branch in the respective region of momentum (Şaşıoğlu et al. 2010). In the direction of increasing momentum, the higher-energy peak grows at the expense of the lower-energy peak, which eventually disappears, and the higher-energy peak then forms the magnon branch. It should be noted, however, that the double-peak structure was observed as two separate peaks in a TDDFT study (Savrasov 1998) and also in a calculation based on a Green-function formulation (Karlsson and Aryasetiawan 2000). The latter study also reported a gapped magnon branch along $\Gamma-\mathrm{L}$ in fcc Ni and a gap around halfway on the line $\Gamma-\mathrm{N}$ in bcc Fe. In fact, there is a gap in this direction in Fig. 8d, albeit at a smaller momentum and energy than in Karlsson and Aryasetiawan (2000). This gap can be attributed to the coupling of the spin-wave branch with a line of increased Stoner intensity. The gapped magnon branch has already been discussed by Blackman et al. (1985) and was observed experimentally (Paul et al. 1988). In conclusion, it remains an open question why the optical branch in fcc Ni appears as a well-defined feature in some calculations, whereas, in others, it is so close to the acoustic branch that the two branches coalesce into a broad peak.

6 Conclusions

We have presented a theoretical method to determine the electronic spin excitations of an interacting many-electron system from first principles. The scheme is based on many-body perturbation theory, in which the spin excitations form the pole structure of the magnetic response function or transverse spin susceptibility. The poles are close to the real-frequency axis, so the imaginary part of the response function yields the corresponding spin excitation spectrum, comprising both single-particle Stoner and collective spin-wave excitations as well as combinations thereof. The latter gives rise to lifetime effects and a redistribution of spectral weight. We have described a very general theoretical derivation, in which the density response function, which is central in describing optical absorption and excitonic effects, appears as a special case.

With the GW approximation for the electronic self-energy, the magnetic response function has been shown to fulfill a Bethe-Salpeter equation, which can be solved in the basis of Wannier product functions. We have sketched a practical implementation in the SPEX code that relies on the full-potential linearized augmented plane-wave method. The screened interaction W is calculated within the RPA. In metallic systems, W falls off very quickly so that we can afford to employ an on-site approximation, i.e., an electron-hole pair is assumed to be on the same site when interacting. In addition, we use the static limit of W for all frequencies, so the screened interaction acts instantaneously. Our implementation allows the magnetic response function to be calculated for arbitrary momenta, which can be used to map the magnetic excitation spectra in very fine detail.

We have studied the long-wavelength limit of the spin-wave spectra for the bulk 3d transition metals Fe, Co, and Ni. The long-wavelength limit is of special interest as the Goldstone theorem demands the existence of a gapless excitation in ferromagnetic materials (neglecting spin anisotropy). Often, this *Goldstone condition* is numerically violated in practical calculations from first principles. We can attribute a large part of this gap error to the approximation of the single-particle Green function. For example, a natural and convenient choice would be the LSDA Green function, which, however, introduces an inconsistency with regard to the theoretical derivation of the Bethe-Salpeter equation. We have proved mathematically that a gapless magnon branch requires the Green function to be self-consistently renormalized with a suitable self-energy, e.g., the COHSEX self-energy, the static limit of the GW approximation. It was shown numerically that the gap error is substantially reduced when using the COHSEX Green function instead of the LSDA one. Furthermore, the self-consistent COHSEX calculations give rise to an overall reduction of the exchange splitting compared to LSDA, often leading to better agreement with experiment. The spin-wave solution of the one-band Hubbard model employing the Hartree-Fock approximation motivates a correction scheme for the LSDA Green function, where the exchange splitting of the Kohn-Sham system is adjusted so as to enforce the Goldstone condition. The resulting spin-wave dispersions are closer to the corresponding COHSEX than to the original

LSDA results. The same can be said about the magnetic moments and exchange splittings obtained from the COHSEX and the corrected LSDA Green function, which are found to be very similar, while the original LSDA values are a bit off. As a result, the corrected LSDA Green function mimics that of the self-consistent COHSEX calculation and is made to fulfill the Goldstone condition exactly, while the numerical cost is identical to a treatment within LSDA. This opens up the possibility of efficient first-principles MBPT calculations of spin excitations that respect the Ward identity of spin conservation.

Spin excitation spectra of the three elementary ferromagnets bcc Fe, fcc Co, and fcc Ni have been calculated and compared to results of model calculations using a spin-polarized homogeneous electron gas. By this comparison, we have shown that the bulk ferromagnets exhibit many features of itinerant-electron magnets that cannot be described by a simple atomic arrangement of magnetic moments, such as in the Heisenberg model. High-energy magnons are strongly damped due to the coupling to single-particle Stoner excitations, and the spin-wave dispersion possesses gaps along certain directions in the Brillouin zone, which can be attributed to a coupling of the spin-wave branch with *Stoner bands*, lines of increased intensity of Stoner excitations.

This coupling effect can be made responsible for the appearance of an *optical branch*, in addition to the acoustic one, in bcc iron. On the other hand, we cannot unambiguously identify an optical branch in fcc nickel along $\Gamma - \mathrm{X}$, which has been much discussed in the literature. While a peak fit of the calculated spin excitation spectrum does reveal two spin-wave peaks at about the right momentum and energy, this appears as a very subtle effect compared to the gaps discussed before. Overall, we find a good agreement of the spin-wave dispersions to neutron scattering experiments.

The present treatment of spin excitations within many-body perturbation theory explicitly describes the correlated motion of an electron-hole pair. This formulation can be straightforwardly extended to yield the dynamical longitudinal spin susceptibility, including its coupling to the charge susceptibility (density response function). Furthermore, it opens up the way for constructing a diagrammatic electronic self-energy that describes the scattering of electrons and holes with magnons, in a similar way as the GW approximation describes the scattering with plasmons. Such a self-energy can be defined by the product of the Green function with the T matrix, yielding the GT self-energy (Hertz and Edwards 1973; Edwards and Hertz 1973). A numerical implementation (Müller 2016; Müller et al. 2019) would be a formidable task given that the T matrix depends on four points in space. It may be possible to combine this self-energy with GW yielding $GW\Gamma$, a self-energy with vertex corrections. Such a self-energy could be able to describe the quasiparticle renormalization (kinks) of electronic bands in magnetic materials due to the scattering with spin fluctuations. It might even shed light on the coupling mechanism in high-temperature superconductors, as it is believed that this coupling arises from the exchange of magnons, through which the effective electron-electron interaction can become attractive.

References

Aryasetiawan F, Karlsson K (1999) Green's function formalism for calculating spin-wave spectra. Phys Rev B 60:7419–7428. https://doi.org/10.1103/PhysRevB.60.7419

Baym G (1962) Self-consistent approximations in many-body systems. Phys Rev 127(4):1391–1401. https://doi.org/10.1103/PhysRev.127.1391

Baym G, Kadanoff LP (1961) Conservation laws and correlation functions. Phys Rev 124(2):287–299. https://doi.org/10.1103/PhysRev.124.287

Blackman JA, Morgan T, Cooke JF (1985) Prediction of high-energy spin-wave excitation in iron. Phys Rev Lett 55:2814–2817. https://doi.org/10.1103/PhysRevLett.55.2814

Bloch F (1930) Zur theorie des ferromagnetismus. Zeitschrift für Physik 61(3):206–219. https://doi.org/10.1007/BF01339661

Bonnenberg D, Hempel K, Wijn H (1986) 3D, 4D and 5D elements, alloys and compounds. In: Wijn HP, Landolt H, Börnstein R (eds) Magnetic properties in metals, new series, vol III. Springer, Berlin. https://doi.org/10.1007/b29710, http://materials.springer.com/bp/docs/978-13-540-39667-3?utm_campaign=bookshelf-experiment&utm_medium=xls&utm_source=staticpage

Brandt U (1971) Modified T-matrix approximation in itinerant ferromagnets. Zeitschrift für Physik 244(3):217–229. https://doi.org/10.1007/BF01395567

Brandt U, Pesch W, Tewordt L (1970) Self-consistent approximations for itinerant ferromagnets above the phase transition point. Zeitschrift für Physik 238(2):121–129. https://doi.org/10.1007/BF01399298

Brandt U, Lustfeld H, Pesch W, Tewordt L (1971) Self-consistent approximations for itinerant ferromagnetism below the phase-transition point. J Low Temp Phys 4(1):79–95. https://doi.org/10.1007/BF00628439

Buczek P (2009) Spin dynamics of complex itinerant magnets. Ph.D. thesis, Martin-Luther-Universität Halle Wittenberg

Buczek P, Ernst A, Bruno P, Sandratskii LM (2009) Energies and lifetimes of magnons in complex ferromagnets: a first-principle study of Heusler alloys. Phys Rev Lett 102:247206. https://doi.org/10.1103/PhysRevLett.102.247206

Buczek P, Ernst A, Sandratskii LM (2010) Standing spin waves as a basis for the control of terahertz spin dynamics: time dependent density functional theory study. Phys Rev Lett 105:097205. https://doi.org/10.1103/PhysRevLett.105.097205

Buczek P, Ernst A, Sandratskii LM (2011) Interface electronic complexes and landau damping of magnons in ultrathin magnets. Phys Rev Lett 106:157204. https://doi.org/10.1103/PhysRevLett.106.157204

Callaway J, Chatterjee AK, Singhal SP, Ziegler A (1983) Magnetic susceptibility of ferromagnetic metals: application to nickel. Phys Rev B 28:3818

Collins MF, Minkiewicz VJ, Nathans R, Passell L, Shirane G (1969) Critical and spin-wave scattering of neutrons from iron. Phys Rev 179:417–430. https://doi.org/10.1103/PhysRev.179.417

Cooke JF (1973) Neutron scattering from itinerant-electron ferromagnets. Phys Rev B 7:1108–1116. https://doi.org/10.1103/PhysRevB.7.1108

Cooke JF (1976) Magnetic excitations in itinerant electron systems. In: Moon RM (ed), Proceedings of the conference on neutron scattering. NTIS, Springfield, VA, 2:723

Cooke JF, Lynn JW, Davis HL (1980) Calculations of the dynamic susceptibility of nickel and iron. Phys Rev B 21:4118–4131. https://doi.org/10.1103/PhysRevB.21.4118

Cooke JF, Blackman JA, Morgan T (1985) New interpretation of spin-wave behavior in nickel. Phys Rev Lett 54:718–721. https://doi.org/10.1103/PhysRevLett.54.718

Dagotto E (1994) Correlated electrons in high-temperature superconductors. Rev Mod Phys 66:763–840. https://doi.org/10.1103/RevModPhys.66.763

Doniach S, Engelsberg S (1966) Low-temperature properties of nearly ferromagnetic Fermi liquids. Phys Rev Lett 17:750–753. https://doi.org/10.1103/PhysRevLett.17.750

Eastman DE, Himpsel FJ, Knapp JA (1980) Experimental exchange-split energy-band dispersions for Fe, Co, and Ni. Phys Rev Lett 44:95–98. https://doi.org/10.1103/PhysRevLett.44.95

Edwards DM, Hertz JA (1973) Electron-magnon interactions in itinerant ferromagnetism. II. Strong ferromagnetism. J Phys F Metal Phys 3(12):2191. http://stacks.iop.org/0305-4608/3/i=12/a=019

Faleev SV, van Schilfgaarde M, Kotani T (2004) All-electron self-consistent *GW* approximation: application to Si, MnO, and NiO. Phys Rev Lett 93:126406. https://doi.org/10.1103/PhysRevLett.93.126406

Freimuth F, Mokrousov Y, Wortmann D, Heinze S, Blügel S (2008) Maximally localized Wannier functions within the FLAPW formalism. Phys Rev B 78:035120. https://doi.org/10.1103/PhysRevB.78.035120

Friedrich C, Blugel S, Schindlmayr A (2009) Efficient calculation of the coulomb matrix and its expansion around k = 0 within the FLAPW method. Comput Phys Commun 180:347

Friedrich C, Blügel S, Schindlmayr A (2010) Efficient implementation of the *GW* approximation within the all-electron FLAPW method. Phys Rev B 81:125102. https://doi.org/10.1103/PhysRevB.81.125102

Friedrich C, Şaşıoğlu E, Müller M, Schindlmayr A, Blügel S (2014) Spin excitations in solids from many-body perturbation theory. In: Di Valentin C, Botti S, Cococcioni M (eds) First principles approaches to spectroscopic properties of complex materials, topics in current chemistry, vol 347. Springer, Berlin/Heidelberg, pp 259–301. https://doi.org/10.1007/128_2013_518

Frikkee E (1966) Inelastic scattering of neutrons by spin waves in F.C.C. cobalt. Physica 32(11):2149–2160

Glinka CJ, Minkiewicz VJ, Passell L (1977) Small-angle critical neutron scattering from cobalt. Phys Rev B 16:4084–4103. https://doi.org/10.1103/PhysRevB.16.4084

Halilov SV, Perlov AY, Oppeneer PM, Eschrig H (1997) Magnon spectrum and related finite-temperature magnetic properties: a first-principle approach. EPL (Europhys Lett) 39(1):91. http://stacks.iop.org/0295-5075/39/i=1/a=091

Hedin L (1965) New method for calculating the one-particle green's function with application to the electron-gas problem. Phys Rev 139:A796–A823. https://doi.org/10.1103/PhysRev.139.A796

Hedin L (1999) On correlation effects in electron spectroscopies and the GW approximation. J Phys Condens Matter 11(42):R489. http://stacks.iop.org/0953-8984/11/i=42/a=201

Hertz JA, Edwards DM (1973) Electron-magnon interactions in itinerant ferromagnetism. I. Formal theory. J Phys F Metal Phys 3(12):2174. http://stacks.iop.org/0305-4608/3/i=12/a=018

Himpsel FJ, Eastman DE (1980) Experimental energy-band dispersions and magnetic exchange splitting for cobalt. Phys Rev B 21:3207–3213. https://doi.org/10.1103/PhysRevB.21.3207

Hofmann A, Cui XY, Schäfer J, Meyer S, Höpfner P, Blumenstein C, Paul M, Patthey L, Rotenberg E, Bünemann J, Gebhard F, Ohm T, Weber W, Claessen R (2009) Renormalization of bulk magnetic electron states at high binding energies. Phys Rev Lett 102:187204. https://doi.org/10.1103/PhysRevLett.102.187204

Hohenberg P, Kohn W (1964) Inhomogeneous electron gas. Phys Rev 136:B864–B871. https://doi.org/10.1103/PhysRev.136.B864

Hong J, Mills DL (1999) Theory of the spin dependence of the inelastic mean free path of electrons in ferromagnetic metals: a model study. Phys Rev B 59:13840–13848. https://doi.org/10.1103/PhysRevB.59.13840

Hong J, Mills DL (2000) Spin dependence of the inelastic electron mean free path in Fe and Ni: explicit calculations and implications. Phys Rev B 62:5589–5600. https://doi.org/10.1103/PhysRevB.62.5589

Janak J (1978) Itinerant ferromagnetism in fcc cobalt. Solid State Commun 25(2):53–55. https://doi.org/10.1016/0038-1098(78)90354-X, http://www.sciencedirect.com/science/article/pii/003810987890354X

Karlsson K, Aryasetiawan F (2000) A many-body approach to spin-wave excitations in itinerant magnetic systems. J Phys Condens Matter 12(34):7617. http://stacks.iop.org/0953-8984/12/i=34/a=308

Khitun A, Wang KL (2005) Nano scale computational architectures with spin wave bus. Superlattice Microst 38(3):184–200. https://doi.org/10.1016/j.spmi.2005.07.001, http://www.sciencedirect.com/science/article/pii/S0749603605000716

Kisker E, Schröder K, Gudat W, Campagna M (1985) Spin-polarized angle-resolved photoemission study of the electronic structure of Fe(100) as a function of temperature. Phys Rev B 31:329–339. https://doi.org/10.1103/PhysRevB.31.329

Kohn W, Sham LJ (1965) Self-consistent equations including exchange and correlation effects. Phys Rev 140:A1133–A1138. https://doi.org/10.1103/PhysRev.140.A1133

Kotani T, van Schilfgaarde M (2008) Spin wave dispersion based on the quasiparticle self-consistent GW method: NiO, MnO and α-MnAs. J Phys Condens Matter 20(29):295214. http://stacks.iop.org/0953-8984/20/i=29/a=295214

Kübler J (2009) Theory of itinerant electron magnetism. International series of monographs on physics. OUP, Oxford. https://books.google.de/books?id=ZbM0gHCcmaQC

Loong CK, Carpenter JM, Lynn JW, Robinson RA, Mook HA (1984) Neutron scattering study of the magnetic excitations in ferromagnetic iron at high energy transfers. J Appl Phys 55(6):1895–1897. https://doi.org/10.1063/1.333511

Lounis S, Costa AT, Muniz RB, Mills DL (2010) Dynamical magnetic excitations of nanostructures from first principles. Phys Rev Lett 105:187205. https://doi.org/10.1103/PhysRevLett.105.187205

Lounis S, Costa AT, Muniz RB, Mills DL (2011) Theory of local dynamical magnetic susceptibilities from the Korringa-Kohn-Rostoker Green function method. Phys Rev B 83:035109. https://doi.org/10.1103/PhysRevB.83.035109

Lowde RD, Moon RM, Pagonis B, Perry CH, Sokoloff JB, Vaughan-Watkins RS, Wiltshire MCK, Crangle J (1983) A polarised-neutron scattering demonstration of deviations from stoner-theory behaviour in nickel. J Phys F Metal Phys 13(2):249. http://stacks.iop.org/0305-4608/13/i=2/a=004

Lynn JW (1975) Temperature dependence of the magnetic excitations in iron. Phys Rev B 11:2624–2637. https://doi.org/10.1103/PhysRevB.11.2624

Mahan GD (2000) Many particle physics, 3rd edn. Plenum, New York

Marzari N, Vanderbilt D (1997) Maximally localized generalized Wannier functions for composite energy bands. Phys Rev B 56:12847–12865. https://doi.org/10.1103/PhysRevB.56.12847

Mermin ND, Wagner H (1966) Absence of ferromagnetism or antiferromagnetism in one- or two-dimensional isotropic Heisenberg models. Phys Rev Lett 17:1133–1136. https://doi.org/10.1103/PhysRevLett.17.1133

Minkiewicz VJ, Collins MF, Nathans R, Shirane G (1969) Critical and spin-wave fluctuations in nickel by neutron scattering. Phys Rev 182:624–631. https://doi.org/10.1103/PhysRev.182.624

Monkhorst HJ, Pack JD (1976) Special points for Brillouin-zone integrations. Phys Rev B 13:5188–5192. https://doi.org/10.1103/PhysRevB.13.5188

Mook HA, Nicklow RM (1973) Neutron scattering investigation of the magnetic excitations in iron. Phys Rev B 7:336–342. https://doi.org/10.1103/PhysRevB.7.336

Mook HA, Paul DM (1985) Neutron-scattering measurement of the spin-wave spectra for nickel. Phys Rev Lett 54:227–229. https://doi.org/10.1103/PhysRevLett.54.227

Mook HA, Tocchetti D (1979) Neutron-scattering measurements of the generalized susceptibility $\chi(q, e)$ for Ni. Phys Rev Lett 43:2029–2032. https://doi.org/10.1103/PhysRevLett.43.2029

Moriya T (1985) Spin fluctuations in itinerant electron magnetism. Springer series in solid state sciences, vol 56. Springer, Berlin/Heidelberg

Moruzzi VL, Marcus PM, Schwarz K, Mohn P (1986) Ferromagnetic phases of bcc and fcc Fe, Co, and Ni. Phys Rev B 34:1784–1791. https://doi.org/10.1103/PhysRevB.34.1784

Müller MCTD (2016) Spin-wave excitations and electron-magnon scattering in elementary ferromagnets from ab initio many-body perturbation theory. Ph.D. thesis, RWTH Aachen

Müller MCTD, Friedrich C, Blügel S (2016) Acoustic magnons in the long-wavelength limit: investigating the goldstone violation in many-body perturbation theory. Phys Rev B 94:064433. https://doi.org/10.1103/PhysRevB.94.064433

Müller MCTD, Blügel S, Friedrich C (2019) Electron-magnon scattering in elementary ferromagnets from first principles: lifetime broadening and kinks. Phys Rev B 100:045130

Paul DM, Mitchell PW, Mook HA, Steigenberger U (1988) Observation of itinerant-electron effects on the magnetic excitations of iron. Phys Rev B 38:580–582. https://doi.org/10.1103/PhysRevB.38.580

Rath J, Freeman AJ (1975) Generalized magnetic susceptibilities in metals: application of the analytic tetrahedron linear energy method to SC. Phys Rev B 11:2109–2117. https://doi.org/10.1103/PhysRevB.11.2109

Raue R, Hopster H, Clauberg R (1984) Spin-polarized photoemission study on the temperature dependence of the exchange splitting of Ni. Zeitschrift für Physik B Condens Matter 54(2):121–128. https://doi.org/10.1007/BF01388063

Rosengaard NM, Johansson B (1997) Finite-temperature study of itinerant ferromagnetism in Fe, Co, and Ni. Phys Rev B 55:14975–14986. https://doi.org/10.1103/PhysRevB.55.14975

Rousseau B, Eiguren A, Bergara A (2012) Efficient computation of magnon dispersions within time-dependent density functional theory using maximally localized Wannier functions. Phys Rev B 85:054305. https://doi.org/10.1103/PhysRevB.85.054305

Runge E, Gross EKU (1984) Density-functional theory for time-dependent systems. Phys Rev Lett 52:997–1000. https://doi.org/10.1103/PhysRevLett.52.997

Sakisaka Y, Rhodin T, Mueller D (1985) Angle-resolved photoemission from Fe(110): determination of E(k). Solid State Commun 53(9):793–799. https://doi.org/10.1016/0038-1098(85)90221-2, http://www.sciencedirect.com/science/article/pii/0038109885902212

Santoni A, Himpsel FJ (1991) Unoccupied energy bands, exchange splitting, and self-energy of iron. Phys Rev B 43:1305–1312. https://doi.org/10.1103/PhysRevB.43.1305

Şaşıoğlu E, Schindlmayr A, Friedrich C, Freimuth F, Blügel S (2010) Wannier-function approach to spin excitations in solids. Phys Rev B 81:054434. https://doi.org/10.1103/PhysRevB.81.054434

Şaşıoğlu E, Friedrich C, Blügel S (2013) Strong magnon softening in tetragonal FeCo compounds. Phys Rev B 87:020410. https://doi.org/10.1103/PhysRevB.87.020410

Savrasov SY (1998) Linear response calculations of spin fluctuations. Phys Rev Lett 81:2570–2573. https://doi.org/10.1103/PhysRevLett.81.2570

Scalapino D (1995) The case for $d_{x^2-y^2}$ pairing in the cuprate superconductors. Phys Rep 250(6):329–365. https://doi.org/10.1016/0370-1573(94)00086-I, http://www.sciencedirect.com/science/article/pii/037015739400086I

Schäfer J, Schrupp D, Rotenberg E, Rossnagel K, Koh H, Blaha P, Claessen R (2004) Electronic quasiparticle renormalization on the spin wave energy scale. Phys Rev Lett 92:097205. https://doi.org/10.1103/PhysRevLett.92.097205

Souza I, Marzari N, Vanderbilt D (2001) Maximally localized Wannier functions for entangled energy bands. Phys Rev B 65:035109. https://doi.org/10.1103/PhysRevB.65.035109

Stearns MB (1986) 3D, 4D and 5D elements, alloys and compounds. In: Wijn H, Landolt H, Börnstein R (eds) Magnetic properties in metals. New series, vol III. Springer, Berlin. https://doi.org/10.1007/b29710, http://materials.springer.com/bp/docs/978-3-540-39667-3?utm_campaign=bookshelf-experiment&utm_medium=xls&utm_source=staticpage

Strinati G (1988) Application of the Green's functions method to the study of the optical properties of semiconductors. La Rivista del Nuovo Cimento 11(12):1–86. https://doi.org/10.1007/BF02725962

Tang H, Plihal M, Mills D (1998) Theory of the spin dynamics of bulk Fe and ultrathin Fe(100) films. J Magn Magn Mater 187(1):23–46. https://doi.org/10.1016/S0304-8853(98)00088-2, http://www.sciencedirect.com/science/article/pii/S0304885398000882

Turner AM, Donoho AW, Erskine JL (1984) Experimental bulk electronic properties of ferromagnetic iron. Phys Rev B 29:2986–3000. https://doi.org/10.1103/PhysRevB.29.2986